Sumoylation-dependent control of Pmk1 phosphorylation during *Magnaporthe oryzae* infection

Caiyun Liu[1,2]*, Hong Hu[2]*, Xuan Cai[2], Jintao Jiang[2], Jing Zheng[2], Ziruo Jiang[2], Yanling Kong[2], Jun Zhu[2], Zhiyong Ren[2], Jing Su[1], Shen Chen[1], Hao Liu[2], Lu Zheng[2], Junbin Huang[2] and Xiao-Lin Chen[2]

[1]Guangdong Provincial Key Laboratory of High Technology for Plant Protection, Plant Protection Research Institute, Guangdong Academy of Agricultural Sciences, Guangzhou, 510640, China; [2]National Key Laboratory of Agricultural Microbiology and Provincial Key Laboratory of Plant Pathology of Hubei Province, College of Plant Science and Technology, Huazhong Agricultural University, Wuhan, 430070, China

Summary

- Rice blast disease, caused by *Magnaporthe oryzae*, significantly threatens global rice yields. The Pmk1-MAPK signaling pathway is crucial for the infection process, but the precise regulatory mechanisms of Pmk1 remain unclear.
- Our research reveals that sumoylation of Pmk1 is vital for its infectious function. A sumoylation site at K347 and two small ubiquitin-related modifier (SUMO)-interacting motifs (SIMs) in Pmk1 are highly conserved across fungi. This sumoylation, orchestrated by Smt3 and Siz1, reduces the phosphorylation of Pmk1 by tuning its interaction with Mst7.
- The Pmk1 sumoylation is high in hyphae and less in conidia, and it intensifies during appressorium maturation. It may act as a molecular brake to prevent excessive Pmk1 phosphorylation during appressorium formation, without affecting phosphatase Pmp1 or the localization of Pmk1. Mutations at K347 lead to hyperphosphorylation of Pmk1 and Mst12, and overexpression of appressorium-related genes. The $\Delta pmk1/Pmk1^{K347R}$ mutant shows deficiencies in storage utilization, turgor accumulation, and septin ring formation.
- Our study highlights the critical role of sumoylation dynamically balancing Pmk1 function via phosphorylation crosstalk, crucial for infection of *M. oryzae*, thus proposing a conserved target for antifungal strategies across fungal pathogens.

Introduction

Rice blast, a disease incited by the fungus *Magnaporthe oryzae*, is one of the most devastating afflictions, persistently endangering the yield and quality of rice crops (Talbot, 2003). To invade plant tissues, *M. oryzae* develops a specialized infection structure known as an appressorium, which employs a pressure-based mechanism to penetrate the lea's rigid cuticle (Dagdas et al., 2012). Multiple signaling pathways are pivotal for the formation and maturation of the appressorium, such as the cAMP-PKA and Pmk1-MAPK pathways (Wilson & Talbot, 2009). Upon entering plant cells, *M. oryzae* develops pseudo-hyphal structures that interact with living host cells, delivering effector molecules to subdue the host's immune response (Giraldo et al., 2013).

The mitogen-activated protein kinase (MAPK) family, conserved from yeast to humans, translates various stimuli into cellular responses. This signaling cascade includes three kinase families, with MAPK kinase kinase (MAPKKK) activating MAPK kinase (MAPKK), which then activates MAPK itself

(Xu, 2000). MAPK pathways influence diverse cellular actions, such as growth, differentiation, stress response, and apoptosis. In fungi, three MAPK proteins similar to *S. cerevisiae*'s Fus3/Kss1, Slt2, and Hog1 are common, with *M. oryzae*'s Pmk1 being the most studied (Turrà et al., 2014). The absence of Fus3/Kss1 homologs typically results in reduced pathogenicity in all tested phytopathogens (Turrà et al., 2014), notably in those that use appressoria for infection (Zhang et al., 2021). *M. oryzae* lacking Pmk1 cannot form appressoria or infect rice, even through wounded leaves. Pmk1 is implicated in lipid and glycogen metabolism during appressorium development, autophagy, cell division, and invasive movement, highlighting its role as a key regulator of the rice blast fungus' pathogenicity (Wilson & Talbot, 2009; Osés-Ruiz et al., 2021; Cruz-Mireles et al., 2024; Zhang et al., 2024).

The regulatory mechanism of Pmk1 is still largely unknown. A recent study in *M. oryzae* reveals that Pmk1-dependent phosphorylation of Mst12 regulates a series of infection-related processes involving septin-dependent cytoskeletal re-organization, exocytosis, and effector gene expression (Osés-Ruiz et al., 2021). Interestingly, our previous study showed that Pmk1 was predicted as a substrate of sumoylation (Liu et al., 2018); however,

*These authors contributed equally to this work.

its experimental evidence is still lacking, and the regulatory significance has not yet been elucidated.

Sumoylation is a key post-translational modification in eukaryotes, involving the attachment of small ubiquitin-related modifiers (SUMO) to proteins (Gareau & Lima, 2010). The process resembles ubiquitination, where a mature SUMO molecule, marked by a C-terminal glycine–glycine (GG) motif, is activated by the E1 enzyme (Aos1/Uba2) and then transferred to the E2 enzyme (Ubc9). Ubc9 conjugates SUMO to specific lysine residues in target proteins, often within a ψKxE/D motif, facilitated by either covalent E2 or E3 regulation or noncovalent SUMO-interacting motif (SIM) interactions (Geiss-Friedlander & Melchior, 2007; Filosa et al., 2013). Unlike ubiquitin, which targets proteins for degradation, sumoylation typically modulates protein interactions, localization, and stability or activity, and is reversible by SUMO proteases, allowing for SUMO recycling (Geiss-Friedlander & Melchior, 2007; Filosa et al., 2013). Proteomic studies have identified numerous SUMO-targeted proteins with a range of biological functions in eukaryotes (Gareau & Lima, 2010). Sumoylation has been implicated in the development and pathogenicity of plant pathogenic fungi, including *M. oryzae* (Liu et al., 2018, 2021; Jian et al., 2023; Shao et al., 2023). Our research has shown that sumoylation is pivotal for appressorium maturation and invasive growth in *M. oryzae* (Liu et al., 2018), but the detailed mechanisms are not fully understood.

In this study, we demonstrated that Pmk1 undergoes sumoylation at K347 by Smt3 and Siz1, which suppresses Pmk1 phosphorylation by influencing its interaction with protein kinase Mst7. This sumoylation acts as a brake mechanism during appressorium formation in *M. oryzae*. The K347R mutation in Pmk1 leads to increased phosphorylation of Pmk1 and Mst12, resulting in hyperphosphorylation of Pmk1 and the formation of two appressoria from one conidium. Additionally, the $\Delta pmk1/Pmk1^{K347R}$ mutant disrupts cellular processes linked to appressorium maturation, causing decreased appressorial penetration. Our findings reveal a novel regulatory mechanism where the Pmk1-MAPK signaling pathway is coordinated by the interplay of sumoylation and phosphorylation. This sumoylation of Pmk1 functions as a crucial brake mechanism for proper phosphorylation during appressorium formation, highlighting its essential role in the infection process of *M. oryzae*.

Materials and Methods

Fungal strains and growth determination

The *Magnaporthe oryzae* wild-type (WT) strain P131 served as the parental strain. Mycelial growth for both P131 and its derivative strains was carried out on Oatmeal Tomato Agar plates at 28°C. Vegetative mycelia for protein and nucleic acid extraction were harvested from a liquid complete medium. Details of all *M. oryzae* transformants used in this study are listed in Table S1, and the plasmids of various genes are listed in Table S2.

Generation of mutations in target protein

To generate the Pmk1^{K347R}, Pmk1$^{\Delta SIM1}$, and Pmk1$^{\Delta SIM2}$ mutant expression vectors, first, the Pmk1 expression plasmid (pGTN-Pmk1) was constructed by amplifying the whole Pmk1 genomic gene with a 1.5-kb region of genomic DNA upstream of the Pmk1 initiator codon, which is known as the Pmk1 native promoter, and then, Pmk1^{K347R}, Pmk1$^{\Delta SIM1}$, and Pmk1$^{\Delta SIM2}$ were amplified from the pGTN-Pmk1 vector using specific primers containing artificially introduced K347R, SIM1, and SIM2 mutations (Table S3). The PCR product was cloned into the pGTN vector to generate pGTN-Pmk1^{K347R}, pGTN-Pmk1-$^{\Delta SIM1}$, and pGTN-Pmk1$^{\Delta SIM2}$ using the Mut Express® II Fast Mutagenesis Kit (Vazyme, Nanjing, China). Using the same method, we also generated pKN-Pmk1^{K347R} for co-transformation with septins in $\Delta pmk1$. Similarly, to generate the Pmk1 expression construct in *Escherichia coli*, the full coding sequences (CDS) of Pmk1 were amplified and cloned into the pGEX4T1 vector labeled as pGST-Pmk1. Next, pGST-Pmk1^{K347R}, pGST-Pmk1-$^{\Delta SIM1}$, and pGST-Pmk1$^{\Delta SIM2}$ expression vectors were constructed. For the yeast two-hybrid (Y2H) assay, the pGBKT7-Pmk1, pGBKT7-Pmk1^{K347R}, pGBKT7-Pmk1^{I85A}, pGBKT7-Pmk1$^{\Delta SIM1}$ and pGBKT7-Pmk1$^{\Delta SIM2}$ vectors were constructed. For Smt3(GG) mutation, we also used specific primers that artificially lost the last alanine to amplify the Smt3 exposed GG motif and then cloned it into the vectors, such as pGADT7 and pGBKT7. All the amplification primers for these mutants are shown in Table S3.

Poly-sumoylation assay *in vivo* and *in vitro*

To determine whether Pmk1 is sumoylated by Smt3 in *M. oryzae*, the pGTN-Pmk1 construct was transformed into both the WT and the $\Delta smt3$ strains. Total protein was extracted from the hyphae of WT/*Pmk1-GFP* and $\Delta smt3$/*Pmk1-GFP* strains. The Pmk1-GFP interacting proteins were purified using anti-GFP nanobody agarose beads (AlpaLifeBio, Shenzhen, China, KTSM1301). The sumoylation status was assessed by western blotting with an anti-SMT3 polyclonal antibody (biorbyt, orb351113), with the anti-GFP antibody (Biodragon, China) serving as a loading control.

For the *in vitro* poly-sumoylation assay, the full-length cDNA of target proteins (Smt3, Pmk1, and its mutants) was cloned into pGEX4T1 to create a GST-tagged target protein construct. The SUMO E1 enzymes (Aos1 and Uba2) and SUMO E2 (Ubc9) were cloned into the pMal-c4X vector, while Smt3 was cloned into pET28a for protein expression. These vectors were transformed into *E. coli* BL21 (WeiDi, Shanghai, China), and the bacteria were grown in Luria-Bertani (LB) liquid medium with appropriate antibiotics at 37°C. At an OD_{600} of 0.5, 0.5 mM IPTG (Beyotime, Shanghai, China) was added to induce protein expression. After a 3-h induction, the *E. coli* cells were centrifuged, resuspended in PBS with PMSF and a protease inhibitor cocktail, and lysed by ultrasonication. Total protein was extracted and the recombinant proteins were purified following the

manufacturer's instructions. The concentration of purified proteins was determined using Coomassie brilliant blue (CBB; Solarbio, Beijing, China) staining.

The *in vitro* sumoylation reaction contained Glutathione S-transferases (GST)-tagged proteins, MBP-tagged proteins with Ubc9 and Aos1/Uba2, His-Smt3, and reaction buffer. As a negative control, the UBC9 inhibitor 2-D08 was added to prevent Smt3 transfer from the Ubc9-SUMO thioester to substrates. This mixture was incubated for 1 h at 37°C. For SUMO chain analysis, purified His-Smt3 was incubated with Ubc9 and Aos1/Uba2, and GST-Pmk1 with its mutants was incubated similarly. Purification of GST-tagged proteins was performed using GST-tag Purification Resin (Solarbio, P2020), and the pull-down proteins were analyzed by western blot with a mouse anti-GST-Tag mAb (Abclonal, Wuhan, China, AE001). CBB staining and His-Tag mouse monoclonal antibody (Coolaber, Beijing, China) western blot served as controls.

Co-immunoprecipitation assay

The pGTN-Pmk1 construct was made as previously reported, and the full-length Smt3 gene was amplified from genomic DNA and cloned into the pKN-Flag vector. Both vectors were co-transformed into the WT P131 strain and also transformed individually. Transformants were selected for G418 resistance and verified using western blot with anti-GFP and anti-Flag antibodies to obtain the strains P131/Pmk1-GFP + Smt3-Flag, P131/Pmk1-GFP, and P131/GFP + Smt3-Flag. Total proteins from the transformants were extracted using a protein lysing buffer (P0013; Beyotime), then incubated with anti-GFP nanobody agarose beads at 4°C overnight. The beads were washed four times with Tris-buffered saline (TBS: 50 mM Tris–HCl, 150 mM NaCl, pH 7.4). Proteins attached to the beads were eluted with 1× protein loading buffer (P0015; Beyotime) after boiling for 5 min and were detected using anti-GFP and anti-Flag antibodies.

Yeast two-hybrid assay

The full-length Pmk1 CDS, with and without mutations at the SUMO site, was cloned into the prey vector pGADT7. Meanwhile, the Smt3 CDS and a modified version, Smt3(GG), exposing the lysine-lysine motif through specific mutagenesis (as detailed in generation of mutations method previously), were cloned into the bait vector pGBKT7. These prey-bait plasmid pairs were co-transformed into the yeast strain Y2H Gold following standard protocols. Transformants were initially selected on synthetic dropout (SD) plates lacking tryptophan and leucine. Positive colonies were then transferred to SD plates lacking tryptophan, leucine, and histidine to assess growth, an indicator of protein–protein interaction (Liu *et al.*, 2022). To prevent self-activation, the SD-Trp-Leu-His medium (Coolaber) was supplemented with inhibitors, such as 25 mM 3-aminotriazole (3-AT; Coolaber) and 100 ng ml^{-1} abscisic acid (ABA; Coolaber). For all the Y2H assays, pGADT7-T and pGBKT7-53 were co-

transformed as a positive control, and pGADT7-T and pGBKT7-Lam were co-transformed as negative controls.

Bimolecular fluorescence complementation assay

The plasmid for Pmk1-nYFP/Pmk1^{K347R}-nYFP was constructed by inserting the Pmk1 or Pmk1^{K347R} gene, driven by its native promoter, into the pHZ65 vector, which carries a hygromycin resistance gene. Separately, the *Smt3*, *Siz1*, and *Mst7* genes, each under their native promoter, were integrated into the pHZ68 vector with a bleomycin resistance gene to create the cYFP plasmid. Both plasmids were then transfected into the protoplasts of the P131 strain. Transformants resistant to both hygromycin and bleomycin were isolated and examined using a laser confocal microscope TCS SP8 (Leica Microsystems, Mannheim, Germany) at an excitation wavelength of 488 nm.

Appressorium formation and collapse assays

To assess appressorium formation, conidial suspensions were adjusted to a concentration of 5×10^4 spores ml^{-1} and applied to a hydrophobic surface. The samples were then incubated in the dark at conditions optimal for *M. oryzae* growth for 24 h. Microscopic examination was conducted to count a minimum of 300 appressoria per strain. Additionally, mature appressoria on the hydrophobic surface were subjected to an 8% glycerol treatment for 30 min, after which the rate of collapsing appressoria was determined.

Pathogenicity tests and infection assay

Leaf spot and spray infection assays were performed on barley and rice leaves to assess the pathogenicity of the *M. oryzae* strain. For rice, a conidial suspension (5×10^4 conidia ml^{-1}) was sprayed onto 2-wk-old seedlings (*Oryza sativa* cv LTH), which were then placed in a chamber at 28°C with 90% humidity for 24 h in the dark, followed by a 12 h : 12 h, light : dark cycle. Lesions were monitored daily and photographed. For barley, 7-d-old leaves (*Hordeum vulgare* cv E9) were sprayed with a conidial suspension (3×10^4 conidia ml^{-1}, 2 ml per leaf), and photographed 5 d post-inoculation. Each test was repeated three times, and leaves were collected for lesion quantification. For infection process observation, a conidial suspension (1×10^5 spores ml^{-1}) was injected into rice sheaths. Inoculated samples were kept in a growth chamber at 28°C and 90% humidity, and the infection process was monitored at various time points using a Nikon Ni90 microscope to observe invasive hyphae penetration and expansion.

Staining assays

Glycogen was visualized using a KI/I$_2$ staining solution containing 60 mg ml^{-1} potassium iodide (KI) and 10 mg ml^{-1} iodine (I$_2$; Thines *et al.*, 2000), while lipid droplets were identified with Nile Red staining. A conidial suspension at a concentration of 5×10^5 conidia ml^{-1} was applied to a hydrophobic surface and

maintained in a growth chamber. The presence of glycogen and lipid droplets was examined at intervals of 0, 2, 4, 6, 8, 12, and 24 h post inoculation (hpi) using an epifluorescence microscope (Ni90; Nikon, Tokyo, Japan).

Phosphorylation assay

Phosphorylated Pmk1 was detected using the Phospho-p44/42 MAPK (Erk1/2; Thr202/Tyr204) antibody (Cell Signaling Technology, Danvers, MA, USA), while the p44/42 MAPK (Erk1/2) antibody (Cell Signaling Technology) was used to detect endogenous Pmk1 expression. For the detection of Mst12 phosphorylation, the Mst12-3 × HA construct was transformed into P131, $\Delta smt3$, and $\Delta pmk1/Pmk1^{K347R}$ strains. Hyphal total protein was analyzed by western blot with anti-HA and anti-GAPDH antibodies. Proteins were separated on 8% sodium dodecyl sulfate - polyacrylamide gel electrophoresis (SDS-PAGE) gels containing 5.0 mM Phos-tag TM AAL and 10 mM $MnCl_2$, run at 20 mA for 4–5 h. Gels were washed three times in buffer with 10 mM ethylenediaminetetraacetic acid (EDTA) for 10 min each, then once without EDTA for 10 min. Proteins were transferred to a polyvinylidene fluoride (PVDF) membrane at 45 V overnight in a 4°C refrigerator. The membrane was probed with anti-HA antibody for western blot analysis. A conventional SDS-PAGE western blot with anti-HA antibody served as a loading control.

For in vitro phosphorylation assays, heterologous production and purification of recombinant pET28a-Flag-MEK2^{DD} was performed as described (Menke et al., 2005), which could activate GST-Pmk1 by incubation in vitro. Recombinant GST-Pmk1/GST-Pmk1^{K347R} (250 ng) and Flag-MEK2^{DD} (250 ng) were incubated in kinase buffer (25 mM Tris pH 7.5, 10 mM MnCl2, 1 mM EGTA, and 2 mM DTT) in the presence of 1 mM ATP at 30°C for 30 min. Phosphorylated Pmk1 was detected as described above.

Analysis of protein interaction predictions

We used the AlphaFold3 tool to predict the structure of interactions between proteins and analyzed the interactions present using PyMol visualization (Abramson et al., 2024).

Statistical analysis

Statistical analyses were performed using the Microsoft Excel 2021 (Microsoft Corp, Washington, DC, USA) or GraphPad Prism 9 (GraphPad Software, Washington, DC, USA). Experimental details, including the number of biological replicates and specific statistical methods, are provided in the corresponding figure legends. All experiments were independently repeated at least three times. For pairwise comparisons, statistical significance was determined by two-sided unpaired Student's t-test, while one-way ANOVA followed by post hoc tests was applied for multiple comparisons. Error bars represent the standard deviation of the mean. Significance levels are indicated as follows: *, $P < 0.05$; **, $P < 0.01$; ***, $P < 0.001$; ****, $P < 0.0001$; and 'ns' denotes no statistical significance.

Result

Pmk1 is dynamically sumoylated during development and infection of M. oryzae

The formation of an appressorium and invasive growth in plants by M. oryzae necessitates a conserved pathogenicity MAPK Pmk1 (Xu & Hamer, 1996; Sakulkoo et al., 2018; Osés-Ruiz et al., 2021). Intriguingly, Pmk1 was identified as a putative SUMO protein in our previous study (Liu et al., 2018). To confirm the sumoylation of Pmk1 in M. oryzae, the hyphae of the Δ pmk1/Pmk1-GFP strains were obtained and used to purify the Pmk1-GFP protein using anti-GFP agarose beads, and then the sumoylation of Pmk1 was detected with an anti-Smt3 antibody. The result indicated that the sumoylation bands of Pmk1 were observed, which could be removed by the SUMO protease (Fig. 1a).

We also evaluated the sumoylation level of Pmk1 in different developmental and infection processes. Total proteins extracted from the hyphae (HY), conidia (CO), and appressoria (AP) of the Δpmk1/Pmk1-GFP strain were also purified by GFP agarose beads and detected by anti-Smt3 antibody. The highest sumoylation level of Pmk1 was found in the hyphae, but it evidently decreased during appressorium maturation (Fig. 1b), suggesting a potential negative regulatory function of sumoylation on Pmk1 during the appressorium and invasive hypha formation.

Sequence analysis revealed that Pmk1 possesses one potential sumoylation site at K347 and two potential SIMs, namely SIM1 (ILDIQ) and SIM2 (ILDVL), which were predicted by the GPS-SUMO online tool (http://SUMOsp.biocuckoo.org/online.php). Furthermore, the sumoylation sites and the potential SIM motifs of Pmk1 are highly conserved in different plant pathogenic fungi (Fig. 1c).

Sumoylation is modified by adding multiple SUMO proteins onto lysine residues. To assess the structural feasibility of the interaction between Pmk1 and the SUMO protein Smt3, molecular docking was conducted based on the structures of Pmk1 and Smt3, as well as E1, E2, and E3. SIMs are hydrophobic small segments of amino acids surrounded by acidic residues, which are arranged in a parallel or antiparallel β-strand. SIMs interact with a hydrophobic pocket on the surface of SUMO (Gareau & Lima, 2010), providing specificity for the interactions of SUMO-conjugated proteins with SUMO poly chains (Song et al., 2004; Kolesar et al., 2012). The interaction between Pmk1 and Smt3 is visualized using AlphaFold3, showing the docking of Smt3 onto the N-terminal region of Pmk1, which exactly happens to Ile85 at the SIM1 site (Fig. 1d), suggesting a potential interaction between Pmk1 and Smt3. Moreover, the structural analysis also indicated that Pmk1 interacted with the E3 ligase Siz1, but did not directly interact with E1 (Aos1/Uba2) and E2 (Uba9; Fig. 1d).

Pmk1 is sumoylated by Smt3

To determine whether the SUMO molecule can be conjugated to substrate proteins in an oligomeric form, we detected the

Fig. 1 Pmk1 is sumoylated in different development stages of *Magnaporthe oryzae*. (a) Western blot analysis of Pmk1 sumoylation in *M. oryzae* hyphae. Sumoylation of Pmk1 was assessed using a small ubiquitin-related modifier (SUMO) protease to degrade the GFP-tagged Pmk1 variant. (b) Developmental stage-specific sumoylation of Pmk1-GFP in *M. oryzae*. Sumoylation levels were examined across various developmental stages. For both A and B, proteins were extracted from the Δ*pmk1*/*Pmk1-GFP* strain, subjected to immunoprecipitation with anti-GFP magnetic beads, and detected using an anti-Smt3 antibody. A reference detection was performed using an anti-GFP antibody. Developmental stages are denoted as follows: CO for conidia, GT for germ tube, AP-4h for appressoria at 4 h post inoculation (hpi) and AP-8h for appressoria at 8 hpi. (c) Conservation of Pmk1 protein structure and sumoylation features. The predicted sumoylation site (S) and SUMO-interacting motifs (SIMs) in Pmk1 of *M. oryzae* are conserved among homologous proteins from different plant pathogenic fungi. The SIMs and sumoylation site are highlighted in red. (d) A structural snapshot of the Pmk1-SUMO components complex model highlighting the docking of Smt3 onto Pmk1 N-terminal region containing the SIM1 site (Ile85) using AlphaFold3. The color labeling of the exact protein is consistent with the color of its protein name, for example, Pmk1 is in green and Smt3 is in blue. An interaction model between Pmk1 (330 Glu) and Siz1 (309 Ser and 311 Ser) is visualized upper. The model below shows the docking of Smt3 onto the N-terminal region of Pmk1, which includes the SIM1 site at Ile85 in red color. In panels (a) and (b), the numbers below each lane represent the normalized Smt3 level relative to Pmk1-GFP abundance.
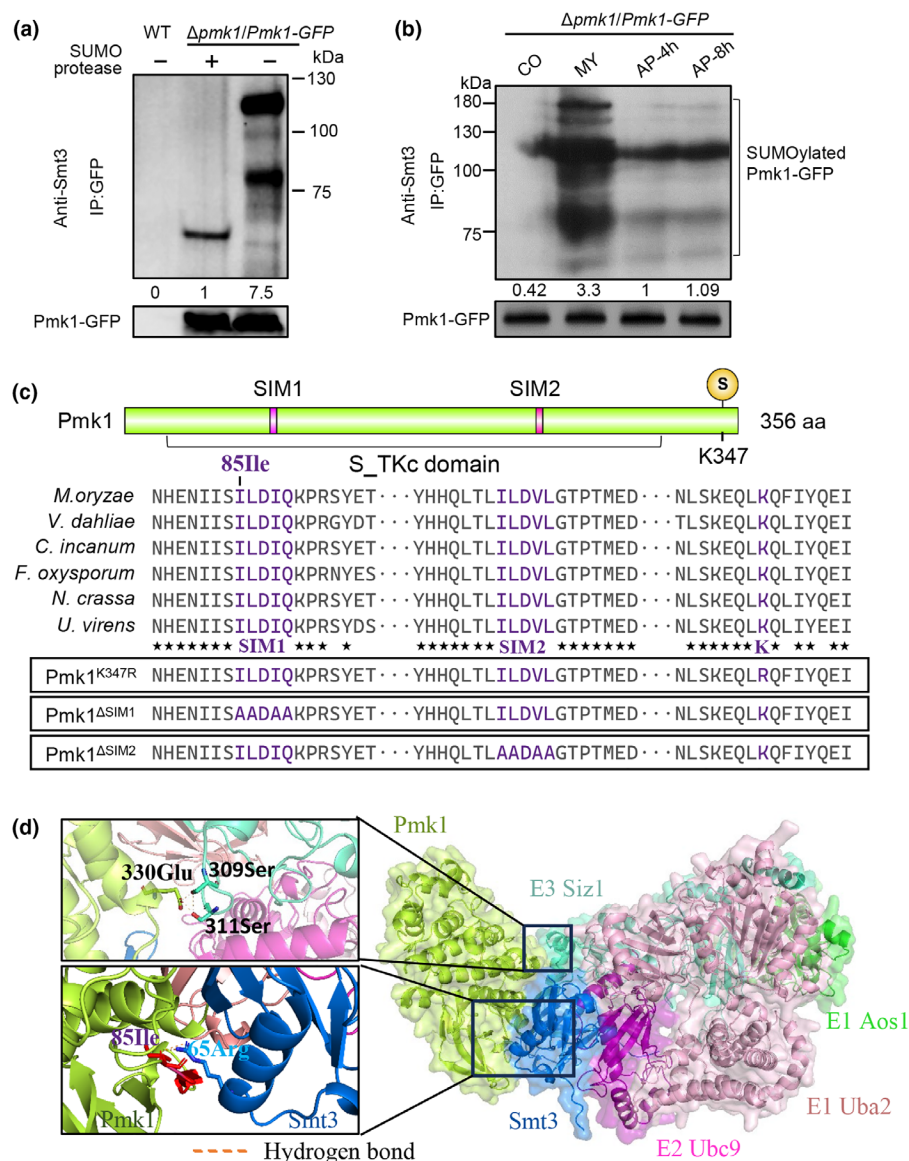
self-polymerization of Smt3. The Y2H assay demonstrated that Smt3 can directly interact with itself when the C-terminal diglycine motif (GG) is exposed, while the interaction is abolished when the motif normally ends with the GGA motif (Fig. 2a), which is the normal ending residue of Smt3. Meanwhile, we transformed Smt3-Flag into P131, and the western blotting analysis revealed that Smt3 can form oligomers, especially dimers in *M. oryzae* (Fig. 2b). Moreover, the GST-Smt3 and other SUMO components, including Aos1-Uba2-MBP and Ubc9-MBP, were expressed in *E. coli* and purified to incubate *in vitro*, and the western blotting analysis using an anti-GST antibody showed that a major GST-Smt3 band along with a series of poly bands were detected, indicating that GST-Smt3 may form a poly chain through self-sumoylation in *M. oryzae* (Fig. 2c).

We further validated the interaction between Smt3 and Pmk1 using *in vivo* and *in vitro* experiments. The Y2H experiment indicated that Pmk1 physically interacts with Smt3 when it harbors

an exposed C-terminal diglycine (GG) motif (Fig. 2d). Additionally, we co-transformed the Smt3-Flag and Pmk1-GFP constructs into the WT strain P131. The resulting strains were then subjected to a co-immunoprecipitation (Co-IP) assay, which confirmed the *in vivo* interaction between Smt3-Flag and Pmk1-GFP (Fig. 2e). Furthermore, we fused nYFP to the N-terminal of Pmk1 and cYFP to the C-terminal of Smt3 and co-transformed these two constructs into the WT strain P131. The bimolecular fluorescence complementation (BiFC) assay showed significant interactions between Pmk1 and Smt3 in hyphae, while their interactions were much weaker in appressoria and conidia (Fig. 2f,g).

To ascertain whether Pmk1 undergoes modification by Smt3 *in vivo*, we introduced the Pmk1-GFP construct into both the WT P131 and the Δ*smt3* mutant strains. The total protein extracts from these strains were subjected to immunoprecipitation using anti-GFP beads, followed by detection with an anti-Smt3 antibody.
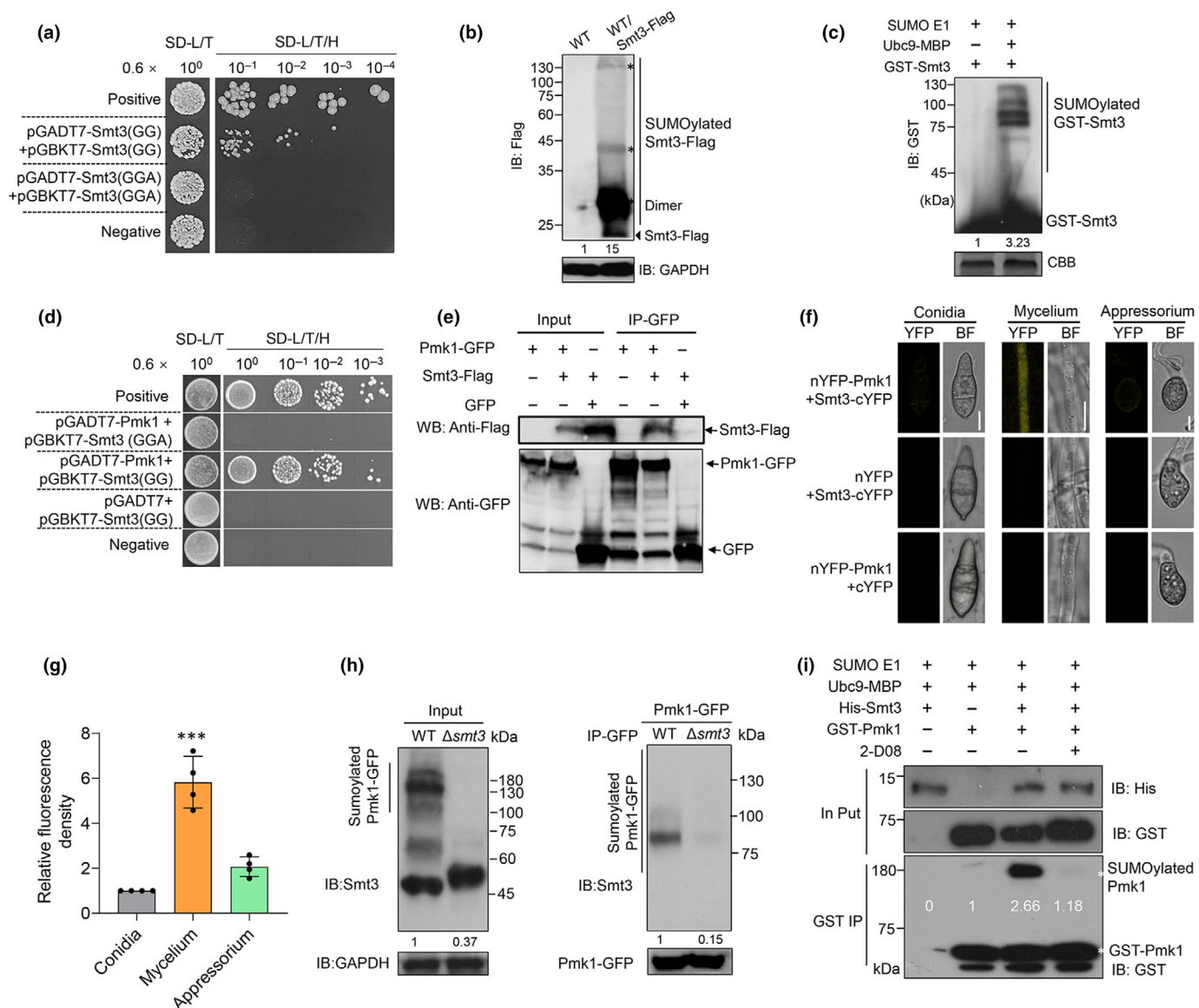
Fig. 2 *In vivo* and *in vitro* sumoylation of Pmk1 by Smt3. (a) Yeast two-hybrid (Y2H) assay of Smt3 self-interaction. Growth on selective synthetic dropout (SD)-L/T/H medium indicates Smt3 self-interaction. Undiluted yeast cells correspond to an OD_{600} = 0.6. Positive controls: pGADT7-T and pGBKT7-P53. Negative controls: pGADT7-T and pGBKT7-Lam. (b) Detection of Smt3 dimerization and small ubiquitin-related modifier (SUMO) chain formation in *Magnaporthe oryzae*. Smt3-Flag presence confirmed by anti-Flag antibody. Anti-GAPDH antibody serves as a loading control. The numbers below each lane represent the normalized Smt3-Flag level relative to GAPDH abundance. (c) *In vitro* self-sumoylation of Smt3. Purified GST-Smt3 was incubated with SUMO E1 and Ubc9-MBP, and detected with an anti-GST antibody. Coomassie brilliant blue (CBB) staining is shown as a loading control. The numbers below each lane represent the normalized GST-Smt3 level relative to CBB abundance. (d) Y2H assay of Smt3-Pmk1 interaction. Interaction confirmed by growth on SD-L/T/H medium. Positive control: pGADT7-T and pGBKT7-53. Negative controls: pGADT7-T with pGBKT7-Lam. (e) Co-immunoprecipitation (Co-IP) of Smt3 and Pmk1. Proteins from *M. oryzae* mycelia were immunoprecipitated with anti-GFP beads and detected with anti-GFP and anti-Flag antibodies. Plasmids expressing GFP and Smt3-Flag, or only expressing Pmk1-GFP, were taken as a negative control. (f) Bimolecular fluorescence complementation assay of Pmk1-Smt3 interaction. nYFP-Pmk1 and Smt3-cYFP cotransformants were observed under confocal microscopy. Negative controls: nYFP with Smt3-cYFP and nYFP-Pmk1 with cYFP. (g) Relative fluorescence density analysis of nYFP-Pmk1 + Smt3-cYFP strains in different stages in (f). Data are presented as mean ± SE from three independent replicates and were analyzed by one-way ANOVA followed by Tukey's test, with asterisks indicating significant differences (***, $P < 0.001$). (h) *In vivo* sumoylation of Pmk1 by Smt3. Pmk1-GFP was expressed in wild-type and Δ*smt3* backgrounds. Sumoylation levels were assessed by anti-Smt3 antibody, with total protein levels as a reference. The numbers below each lane indicate the normalized Smt3 levels relative to the abundance of GAPDH and Pmk1-GFP. (i) *In vitro* sumoylation of Pmk1. Components were incubated at 37°C, and the reaction was purified and immunoblotted with anti-GST and anti-His antibodies. Controls included 2-D08 treatment and reactions with one missing component to confirm sumoylation requirements. The numbers below each lane indicate the relative grayscale values of the SUMOylated Pmk1 bands.

Fig. 3 Essential lysine site and small ubiquitin-related modifier (SUMO)-interacting motifs (SIM) for Pmk1 sumoylation. (a) Yeast two-hybrid assay of Pmk1-Smt3 interaction via SIM1. Growth on synthetic dropout (SD)-L/T/H medium indicates interaction via the SIM1 motif. Undiluted yeast cells correspond to an $OD_{600} = 0.6$. Positive control: pGADT7-T and pGBKT7-P53. Negative control: pGADT7-T and pGBKT7-Lam. (b) *In vivo* analysis of Pmk1 sumoylation mediated by lysine 347 and SIM1. Proteins from $\Delta pmk1$ strains expressing various Pmk1-GFP variants were purified using anti-GFP beads and detected with an anti-SMT3 antibody. Anti-GFP antibody served as a loading control. The numbers below each lane indicate the normalized Smt3 levels relative to the abundance of Pmk1-GFP. (c) *In vitro* sumoylation of Pmk1 variants. Lysine 347 and SIM1 were tested for their role in sumoylation using purified components. Reactions were incubated at 37°C, purified using GST-tag resin, and immunoblotted with an anti-GST antibody. Negative controls omitted either His-Smt3 or GST-Pmk1. The numbers below each lane indicate the relative grayscale values of the SUMOylated Pmk1 bands.

The western blot analysis uncovered a prominent band indicative of Pmk1 sumoylation, which aligned with the anticipated size of multiple Smt3 molecules in the WT/Pmk1-GFP strain. This finding points toward a poly-sumoylation event of Pmk1. Conversely, the $\Delta smt3$ mutant exhibited a markedly diminished level of Pmk1 sumoylation (Fig. 2h).

To further validate the sumoylation of Pmk1 *in vitro*, we expressed and purified the SUMO E1 enzyme complex (Aos1-Uba2-MBP), E2 enzyme (Ubc9-MBP), His-tagged Smt3, and the substrate GST-Pmk1 individually in *E. coli*. The western blot experiment demonstrated that poly-sumoylated GST-Pmk1 was detectable when His-Smt3 and GST-Pmk1 were co-incubated with the purified E1 (Aos1-Uba2) and E2 (Ubc9) enzymes. This sumoylation was notably absent in the negative control lacking SUMO E2 enzyme Ubc9 or when treated with 2-D08, a distinctive inhibitor of protein sumoylation (Fig. 2i). Collectively, these results substantiate that Pmk1 is poly-sumoylated by Smt3 in *M. oryzae*.

E3 ligase Siz1 is required for sumoylation of Pmk1

Sumoylation typically necessitates the facilitation of a SUMO E3 ligase for *in vivo* modification. Given that Siz1 has been recognized as a pivotal E3 ligase for sumoylation in *M. oryzae* (Liu *et al.*, 2018), we investigated its potential role in the recognition and facilitation of Pmk1 sumoylation. The interaction between Pmk1 and Siz1 was examined through both *in vivo* and *in vitro* experiments. The Y2H assay indicated no direct interaction between Pmk1 and Siz1 (Supporting Information Fig. S1a). However, the BiFC assay demonstrated that Pmk1 interacts with Siz1 at various stages of the infection process (Fig. S1b). To explore the necessity of Siz1 for Pmk1 modification *in vivo*, we conducted an experiment where the Pmk1-GFP construct was integrated into both WT P131 and $\Delta siz1$ mutant strains.

Proteins from these strains were extracted and underwent immunoprecipitation with anti-GFP beads, subsequently probed with an anti-Smt3 antibody. The subsequent western blot analysis revealed a significant band corresponding to the sumoylation of Pmk1, matching the expected size for multiple Smt3 attachments in the WT/Pmk1-GFP strain, suggesting extensive poly-sumoylation of Pmk1. By contrast, the $\Delta siz1$ mutant displayed a significant reduction in Pmk1 sumoylation levels (Fig. S1c). Additionally, to predict the spatial distance between Pmk1 and Siz1 protein during the Pmk1 sumoylation process using Alphafold3, the result showed that hydrogen bonds (Glu330 on Pmk1, Ser309, and Ser311 on Siz1) could be formed between Pmk1 and Siz1 proteins in terms of spatial distance (Fig. 1d). The above all indicate that there is no direct interaction between Pmk1 and Siz1, but they may be very spatially close and interact through a third party, thus finishing the sumoylation of Pmk1 with the assistance of the E3 ligase Siz1.

Pmk1 is sumoylated at K347 with the assistance of SIM1 and SIM2 domains

To verify the sumoylation site of Pmk1 at lysine 347 and to elucidate its functional significance, we engineered a mutation converting lysine 347 to arginine, yielding the $Pmk1^{K347R}$ variant. In parallel, to ascertain the roles of the SIM1 and SIM2 motifs, we introduced mutations in their conserved sequences: ILDVQ was altered to AADAA in $Pmk1^{\Delta SIM1}$, and ILDVL was changed to AADAA in $Pmk1^{\Delta SIM2}$ (Fig. 1c). Y2H assays indicated that the $Pmk1^{\Delta SIM1}$ mutants lacked interaction with Smt3, whereas the $Pmk1^{K347R}$ and $Pmk1^{\Delta SIM2}$ mutants retained this physical interaction (Fig. 3a), indicating that SIM1 is probably the key functional interacting motif. Structural analysis showed that Ile85 of Pmk1 within the SIM1 domain could be important for

Pmk1 and Smt3 interaction (Fig. 1c,d). To further validate this interaction pattern, we conducted additional Y2H assays with Pmk1^{I85A}. The results showed that mutating Ile85 in the SIM1 motif significantly weakened the interaction between Pmk1 and Smt3 (Fig. S2), confirming its critical role in Pmk1 and Smt3 interaction. Furthermore, we generated strains expressing Pmk1-GFP, Pmk1^{K347R}-GFP, Pmk1$^{\Delta SIM1}$-GFP, and Pmk1$^{\Delta SIM2}$-GFP with its native promoter by transforming the respective constructs into the $\Delta pmk1$ strain. Total protein extracts from the hyphae of these strains were subjected to immunoprecipitation using anti-GFP agarose beads. Western blotting analysis with an anti-Smt3 antibody revealed that the $\Delta pmk1/Pmk1^{K347R}$-GFP and $\Delta pmk1/Pmk1^{\Delta SIM1}$-GFP strains displayed a substantial decrease in sumoylation signals relative to the $\Delta pmk1/Pmk1$-GFP control. The $\Delta pmk1/Pmk1^{\Delta SIM2}$-GFP strain also exhibited a notable reduction in sumoylation levels (Fig. 3b). These findings underscore that the K347 residue of Pmk1 was probably the sumoylation site, as well as SIM1 was much more important for Pmk1 interaction with Smt3 than SIM2, but this does not exclude that SIM2 was functional.

To further examine the function of the K347 site and SIMs in the Pmk1 sumoylation process, we expressed and purified the recombinant proteins GST-Pmk1, GST-Pmk1^{K347R}, GST-Pmk1$^{\Delta SIM1}$, and GST-Pmk1$^{\Delta SIM2}$ in *E. coli*. As described previously, these purified proteins were individually incubated with the SUMO E1 enzyme complex (Aos1/Uba2-MBP), E2 enzyme (Ubc9-MBP), and His-Smt3 at 37°C for 1 h. Subsequent western blot analysis demonstrated that an evident sumoylation band was exclusively observed in the mixture containing GST-Pmk1, while only a very weak band was detected in the mixture containing GST-Pmk1$^{\Delta SIM2}$. By contrast, no sumoylation was detected in mixtures with GST-Pmk1^{K347R} and GST-Pmk1$^{\Delta SIM1}$ (Fig. 3c). These results collectively suggest that Pmk1 is sumoylated at lysine 347 and that this modification is reliant on the presence of functional SIM1 and SIM2 motifs, in which SIM1 takes a major role.

Sumoylation inhibits phosphorylation of Pmk1

In order to determine whether sumoylation affects the function of Pmk1, we tested the effects of sumoylation on protein stability, subcellular localization, and phosphorylation. Protein level detection experiments by western blot showed that sumoylation did not affect protein stability or degradation of Pmk1, because the protein content of Pmk1-GFP in $\Delta pmk1/Pmk$-GFP, $\Delta pmk1/Pmk1^{K347R}$-GFP, $\Delta pmk1/Pmk1^{\Delta SIM1}$-GFP, $\Delta pmk1/Pmk1^{\Delta SIM2}$-GFP, and $\Delta smt3/Pmk1$-GFP strains was almost the same (Fig. 4a). We then detected whether the phosphorylation level of Pmk1 was affected by sumoylation. Previous studies have shown that Pmk1 activation precedes infection-related development but is maintained throughout appressorium morphogenesis (Cruz-Mireles *et al.*, 2024). The Pmk1 phosphorylation level in WT, $\Delta pmk1/Pmk1$, $\Delta pmk1/Pmk1^{K347R}$, and $\Delta smt3/Pmk1$ strains was detected with a phospho-p42/44 antibody, which is specific to MAP kinases Pmk1 and Mps1 (Li *et al.*, 2017); meanwhile, a p44/42 MAPK (Erk1/2) antibody was used to standardize the expression level of Pmk1. It is shown that during the formation of appressorium, Pmk1 is phosphorylated within 4 h of conidial germination on a hydrophobic surface both in $\Delta pmk1/Pmk1$ and $\Delta pmk1/Pmk1^{K347R}$ strains (Fig. S3). In mycelium, the results showed that, compared with those in $\Delta pmk1/Pmk1$ and the WT, the phosphorylation level of Pmk1 was significantly increased in $\Delta pmk1/Pmk1^{K347R}$ and $\Delta smt3/Pmk1$ (Fig. 4b), suggesting that sumoylation probably suppressed the phosphorylation of Pmk1. To further verify this hypothesis, we performed sumoylation and phosphorylation of Pmk1 *in vitro*. First of all, we used a recombinant constitutively active MAPKK from tobacco (*Nicotiana tabacum*) NtMEK2^{DD} to activate Pmk1, as previously shown (Menke *et al.*, 2005), revealing that both Pmk1 and Pmk1^{K347R} could be phosphorylated in the presence of NtMEK2^{DD} in kinase reaction buffer (Fig. 4c). In this case, we further observed that the phosphorylation of Pmk1 was progressively enhanced, while its sumoylation was correspondingly weakened (Fig. 4d).

Fig. 4 Regulation of Pmk1 function by sumoylation at K347. (a) Protein stability of Pmk1-GFP in wild-type, $\Delta smt3$, and $\Delta pmk1/Pmk1_{K347R}$ strains was assessed using an anti-GFP antibody. Anti-GAPDH antibody was taken as a control. (b) Phosphorylation levels of Pmk1 in the same strains were detected using an anti-P42/44 antibody, with anti-Pmk1 antibody specifically for *Magnaporthe oryzae* as a control. (c) Phosphorylation assays of Pmk1 activated by NtMEK2$_{DD}$ *in vitro*. Purified NtMEK2$_{DD}$ and GST-Pmk1 were co-cultivated in reaction buffer to perform phosphorylation. Phosphorylation levels were detected as mentioned above. (d) Phosphorylation and sumoylation levels detection of Pmk1 *in vitro*. Phosphorylation and sumoylation assays were performed in functional reaction buffer to detect the interaction of these two modifications. The SUMOylation level of Pmk1 was evaluated using anti-GST antibody, while its phosphorylation level was evaluated using Anti-P44/42 antibody. (e) Co-immunoprecipitation assays confirm the interaction between Mst7 and Pmk1 sumoylation mutations. Proteins from *M. oryzae* mycelia were immunoprecipitated with anti-Flag beads and detected with anti-HA and anti-Flag antibodies. (f) Yeast two-hybrid assay demonstrates the interaction between Mst7 and Pmk1 sumoylation mutations. Growth on SD-L/T/H medium indicates interaction, with pGADT7-T and pGBKT7-53 as a positive control, and pGADT7-T and pGBKT7-Lam as negative controls. Undiluted yeast cells correspond to an OD$_{600}$ = 0.6. (g) BiFC assay shows the interaction between Mst7 and Pmk1 sumoylation mutations at the cellular level. Co-transformants were observed under confocal microscopy, with several negative controls included. (h) Relative fluorescence density analysis comparing nYFP-Pmk1+Mst7-cYFP strains and nYFP-Pmk1$_{K347R}$+Mst7-cYFP strains in different stages in (g). Data represent means and standard errors from three replicates, with asterisks indicating significant differences (**, $P < 0.01$; ***, $P < 0.001$). (i) Yeast two-hybrid assay for the interaction between Pmp1 and Pmk1 sumoylation mutations, with additional 25 mM 3-AT and 100 ng ml^{-1} ABA to inhibit self-activation of pGADT7 and pGBKT7-Pmp1 control. Positive and negative controls are as described in (f). (j) Co-immunoprecipitation assays for the interaction between Pmp1 and Pmk1 sumoylation mutations, using the same method as in (e). (k) BiFC assay for the interaction between Pmp1 and Pmk1 sumoylation mutations, with the same imaging conditions and controls as in (g). (l) Relative fluorescence density analysis comparing nYFP-Pmk1+Pmp1-cYFP strain and nYFP-Pmk1$_{K347R}$+Pmp1-cYFP strain in different stages in (k). Data represent means and standard errors from three replicates, with asterisks indicating significant differences (*, $P < 0.05$; **, $P < 0.01$; ***, $P < 0.001$).
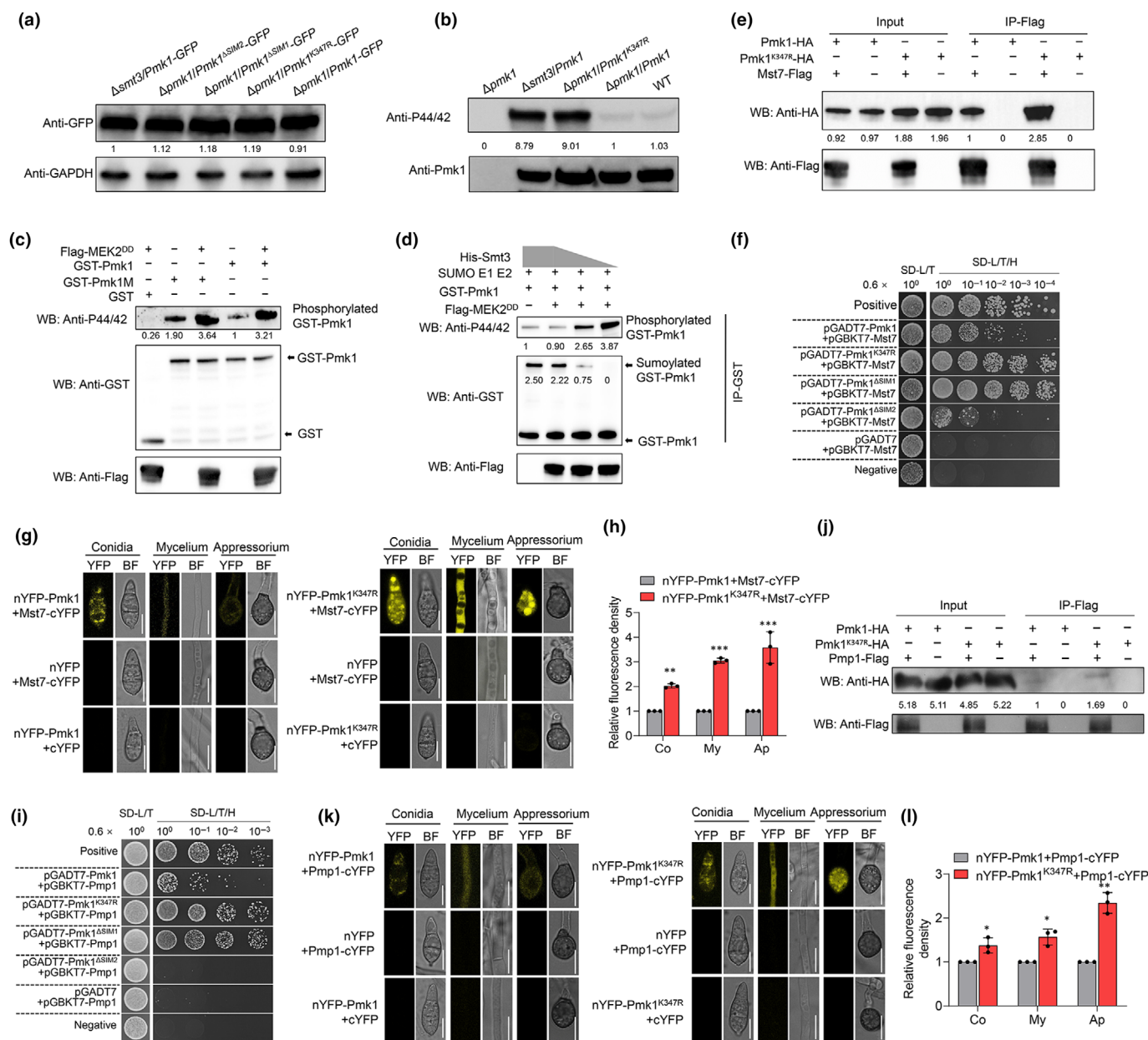
These results collectively suggest that sumoylation would suppress the phosphorylation of Pmk1.

Sumoylation of Pmk1 prevents its interaction with protein kinase Mst7

The Mst11-Mst7-Pmk1 cascade is central in the Pmk1-MAPK signaling pathway and is essential for appressorium formation in *M. oryzae* (Osés-Ruiz *et al.*, 2021). We wonder whether sumoylation could affect the interaction between Pmk1 and Mst7, thereby influencing Pmk1's phosphorylation status. To test this possibility, the Co-IP experiments were performed to determine the interaction strength between Pmk1-HA and Mst7-Flag, as

well as Pmk1^{K347R}-GFP and Mst7-Flag, revealing an enhanced interaction between Pmk1^{K347R} and Mst7 compared with the interaction in Pmk1 and Mst7 (Fig. 4e). The Y2H assays also revealed that the interaction between Pmk1 and Mst7 was significantly enhanced by the K347R mutation and SIM1 mutation in Pmk1, while the SIM2 mutation of Pmk1 maintained its weak interaction with Mst7 (Fig. 4f). Similar results were obtained in conidia, despite the relatively weak interaction between the two proteins in this context (Fig. S4a). Additionally, under *in vitro* sumoylation conditions, the interaction between Pmk1^{K347R} and Mst7 was also found to be enhanced compared with that between Pmk1 and Mst7 (Fig. S4b). Combining these results suggests that the suppressed sumoylation of Pmk1 caused by the specific lysine
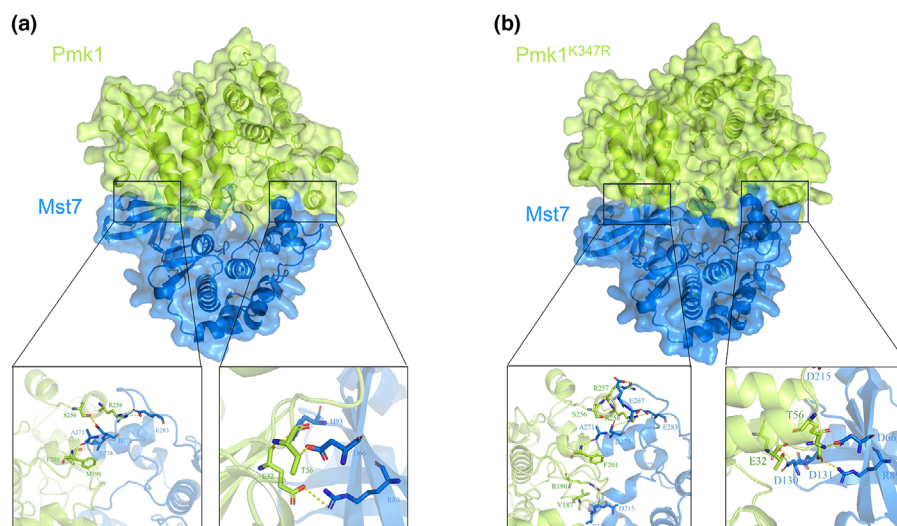
Fig. 5 AlphaFold3-predicted structural molecular docking of Pmk1 and its sumoylation-deficient mutant Pmk1^{K347R} with Mst7. (a) Molecular docking of wild-type (WT) Pmk1 and Mst7. The docking illustrates the precise binding mode and interface between the two proteins, with a focus on selected regions. (b) Molecular docking of Pmk1^{K347R} and Mst7. The docking illustrates the predicted structural interaction between the Pmk1 mutant Pmk1^{K347R} and Mst7. The alteration at the sumoylation site is expected to affect the binding interface, and selected regions with changes in the interaction bonds are highlighted. Both (a) and (b) detail the interaction bonds within the selected regions of the Pmk1-Mst7 and Pmk1^{K347R}-Mst7 complexes. The comparison provides insights into the impact of the K347R mutation on the molecular interface and the stability of the protein–protein interaction.

residue or SIM1 site mutation is intricately linked to the binding affinity between Pmk1 and Mst7.

Further validation was achieved using a BiFC assay. This experiment demonstrated that the strains co-expressing Mst7-cYFP and nYFP-Pmk1^{K347R} exhibited enhanced bright yellow fluorescence across various developmental stages, indicative of a robust interaction. By contrast, this fluorescence was weakly observed in strains expressing Mst7-cYFP and nYFP-Pmk1, which lack the K347R mutation (Fig. 4g,h). These results imply that the K347R mutation significantly influences the interaction between Pmk1 and Mst7, potentially during the infection process of *M. oryzae*.

Sumoylation prevents interaction of Pmk1 with phosphatase Pmp1

The phosphatase Pmp1 is recognized as a negative regulator within the Pmk1-MAPK signaling pathway, playing a pivotal role in modulating its activity in *M. oryzae*. Our investigation postulates that sumoylation, while not directly hindering phosphorylation, may impede the interaction between Mst7 and Pmk1, thus potentially creating an opportunity for Pmp1 to engage with Pmk1 and execute dephosphorylation. To scrutinize this hypothesis, the Y2H assays were conducted, yielding unexpected results: the interaction between Pmp1 and the Pmk1^{K347R} variant was considerably more pronounced than that between Pmp1 and Pmk1 (Fig. 4i). The *in vivo* observations corroborate the notion that sumoylation suppresses the interaction between Pmp1 and Pmk1, rather than promoting it (Fig. 4j).

Further substantiation of our findings was obtained through a BiFC assay. This technique revealed that strains co-expressing

Pmp1 fused to the C-terminal of yellow-fluorescent protein (YFP) (Pmp1-cYFP) and the N-terminal of YFP fused Pmk1^{K347R} (nYFP-Pmk1^{K347R}) displayed intensified bright yellow fluorescence throughout multiple developmental phases. This fluorescence is a strong indicator of an enhanced interaction between the two proteins. Conversely, in strains expressing the WT Pmp1-cYFP and nYFP-Pmk1 without the K347R mutation, the fluorescence signal was significantly diminished (Fig. 4k,l). Therefore, SUMO simultaneously inhibits both phosphorylation and dephosphorylation processes, affecting the kinase and phosphatase interactions with Pmk1.

Structural analysis showed stronger interaction between Pmk1^{K347R} and Mst7

To further elucidate the impact of sumoylation on the interaction between Pmk1 and Mst7, we utilized AlphaFold 3 to predict the spatial interaction structure of both the Pmk1-Mst7 complex and Pmk1^{K347R}-Mst7 complex. Our findings revealed a significant increase in the number of interacting residues between Pmk1^{K347R}-Mst7 complex compared with the Pmk1-Mst7 complex. Specifically, the K347R mutation appears to subtly alter the conformation of Pmk1, thereby facilitating a closer spatial approximation between Pmk1 and Mst7. For example, compared with Pmk1, the mutant Pmk1K347R exhibited tighter hydrogen bonds between its amino acid residues S256, R257, and R258 and D275, E267, and E283 of Mst7, indicating a stronger interaction (Fig. 5a,b). These discoveries imply that sumoylation at K347 might prevent the phosphorylation of Pmk1 by disrupting the interaction interface between Mst7 and Pmk1. This disruption could, in turn, affect the signaling cascade downstream of
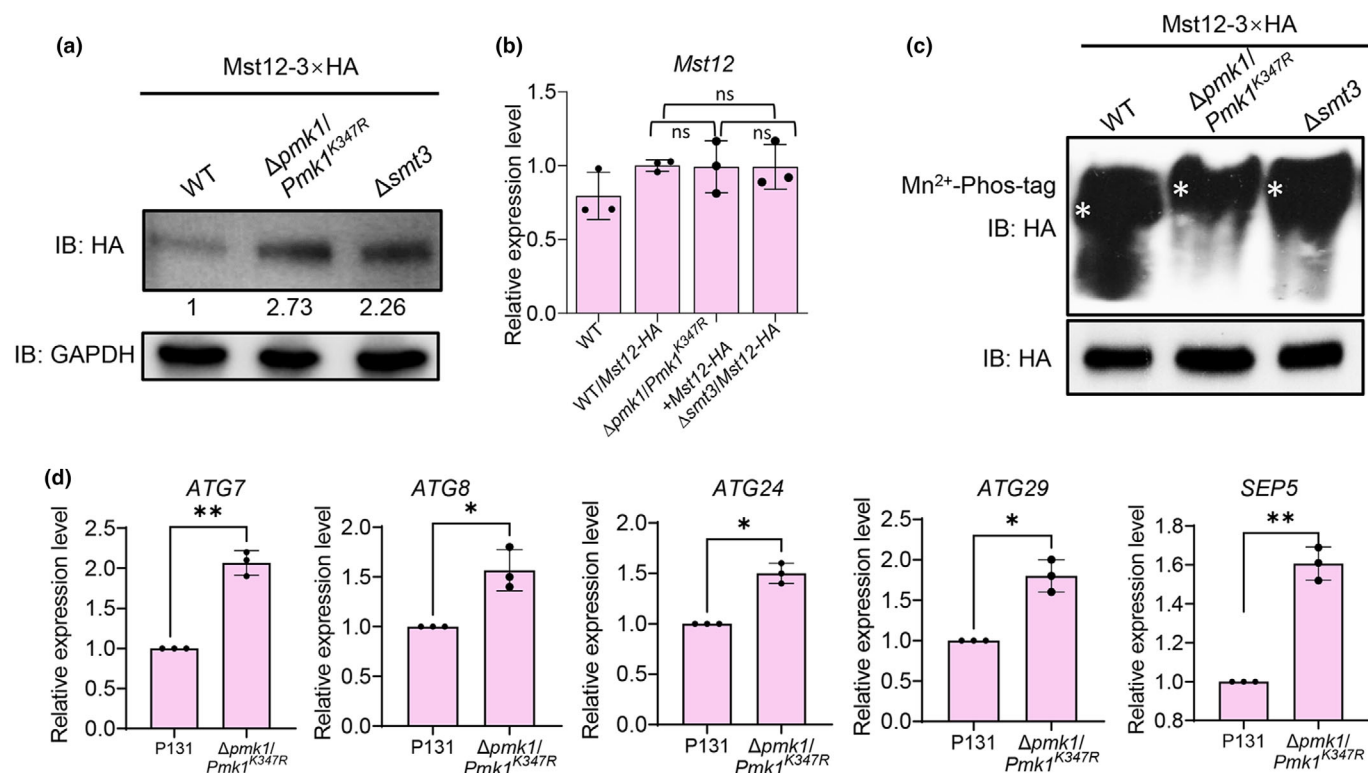
Fig. 6 Phosphorylation of the *Magnaporthe oryzae* Pmk1 target Mst12 is increased in Δ*smt3* and Δ*pmk1/Pmk1*^{K347R}. (a) Protein level of Mst12-3×HA in WT, Δ*smt3*, and Δ*pmk1/Pmk1*^{K347R} strains. Mst12-3×HA was introduced into each strain to assess the impact of the respective mutations on Mst12-3×HA expression levels. The numbers below each lane indicate the relative quantitative value of the HA level. (b) Relative expression level of Mst12-3×HA in WT, Δ*smt3*, and Δ*pmk1/Pmk1*^{K347R} strains. Data are presented as mean ± SE from three independent replicates and were analyzed by one-way ANOVA followed by Tukey's test, ns, no significance. (c) Phosphorylation level of Mst12 in hyphae. After transformation with Mst12-3×HA into WT, Δ*smt3*, and Δ*pmk1/Pmk1*^{K347R} strains, total proteins were treated with a phosphatase inhibitor and separated using Mn^{2+}-Phos-tag SDS-PAGE for phosphorylated species and normal SDS-PAGE. Proteins were then immunoblotted with an anti-HA antibody to detect phosphorylated forms of Mst12-3×HA. (d) Expression level of appressoria-related genes in the wild type strain P131 and Δ*pmk1/Pmk1*^{K347R}. The figure shows the relative expression levels of genes involved in autophagy and septin ring formation, comparing the wild type strain P131 with the Δ*pmk1/Pmk1*^{K347R} strain to evaluate the effect of Pmk1 sumoylation on the transcription of these genes. Data represent means and standard errors from three replicates, with asterisks indicating significant differences (*, $P < 0.05$; **, $P < 0.01$).

the Pmk1-MAPK pathway, which is particularly crucial for various biological processes in *M. oryzae*.

Phosphorylation of the Pmk1 target Mst12 is increased in Δ*smt3* and Δ*pmk1/Pmk1*^{K347R}

Pmk1 can phosphorylate its downstream transcription factor Mst12, thereby regulating gene functions related to septin-dependent cytoskeletal re-organization and polarized exocytosis (Osés-Ruiz *et al.*, 2021). To evaluate the influence of Pmk1 sumoylation on its downstream transcription factor Mst12, we detected the phosphorylation level of Mst12 through a Phos-tag assay. The total proteins of the hyphae in Δ*pmk1/Pmk1*, Δ*pmk1/Pmk1*^{K347R}, and Δ*smt3/Pmk1* were extracted. Western blotting analysis indicated that the protein content of Mst12-3 × HA is higher in Δ*smt3* and Δ*pmk1/Pmk1*^{K347R} than in the WT in the case of the consistent expression level of Mst12 (Fig. 6a), without any difference in transcription levels (Fig. 6b). Additionally, the phosphorylation level of Mst12-3 × HA on polyacrylamide SDS-PAGE gels with Phos-tag is much stronger in Δ*smt3* and Δ*pmk1/Pmk1*^{K347R} than in Δ*pmk1/Pmk1* (Fig. 6c),

confirming that the inhibition of phosphorylation in Pmk1 caused by sumoylation affected the phosphorylation of its downstream target.

Further quantitative reverse transcription polymerase chain reaction (qRT-PCR) analysis revealed that the expression of some downstream targets reported to be activated by Pmk1, including *ATG7*, *ATG8*, *ATG24*, *ATG29*, and *SEP5*, was significantly increased in the Δ*pmk1/Pmk1*^{K347R} mutants (Cruz-Mireles *et al.*, 2024), such as *ATG* and *SEP* genes (Fig. 6d). The collective findings indicate that sumoylation of Pmk1 at the K347 residue negatively regulates its kinase activity, leading to decreased phosphorylation of the downstream transcription factor Mst12 and altered expression of Pmk1-activated genes, which in turn impacts key cellular processes and pathogenicity in *M. oryzae*.

Localization of Pmk1 is not affected by sumoylation

M. oryzae Pmk1 is found to be a key regulator of downstream transcription factors for regulating the expression of global genes during infection. It seems to accumulate in the nucleus to phosphorylate some transcriptional factors that are essential for

appressorium maturation (Bruno *et al.*, 2004; Osés-Ruiz *et al.*, 2021). We then investigated whether the subcellular localization of Pmk1 is influenced by sumoylation. The subcellular localization of Pmk1 was observed in the strains of $\Delta pmk1/$

$Pmk1$-GFP, $\Delta pmk1/Pmk1^{K347R}$-GFP, and $\Delta smt3/Pmk1$-GFP. We discovered that the percentage of nuclear-localized Pmk1 did not appear to be significantly affected in both $\Delta pmk1/Pmk1^{K347R}$-GFP and $\Delta smt3/Pmk1$-GFP (Fig. S5a–c),
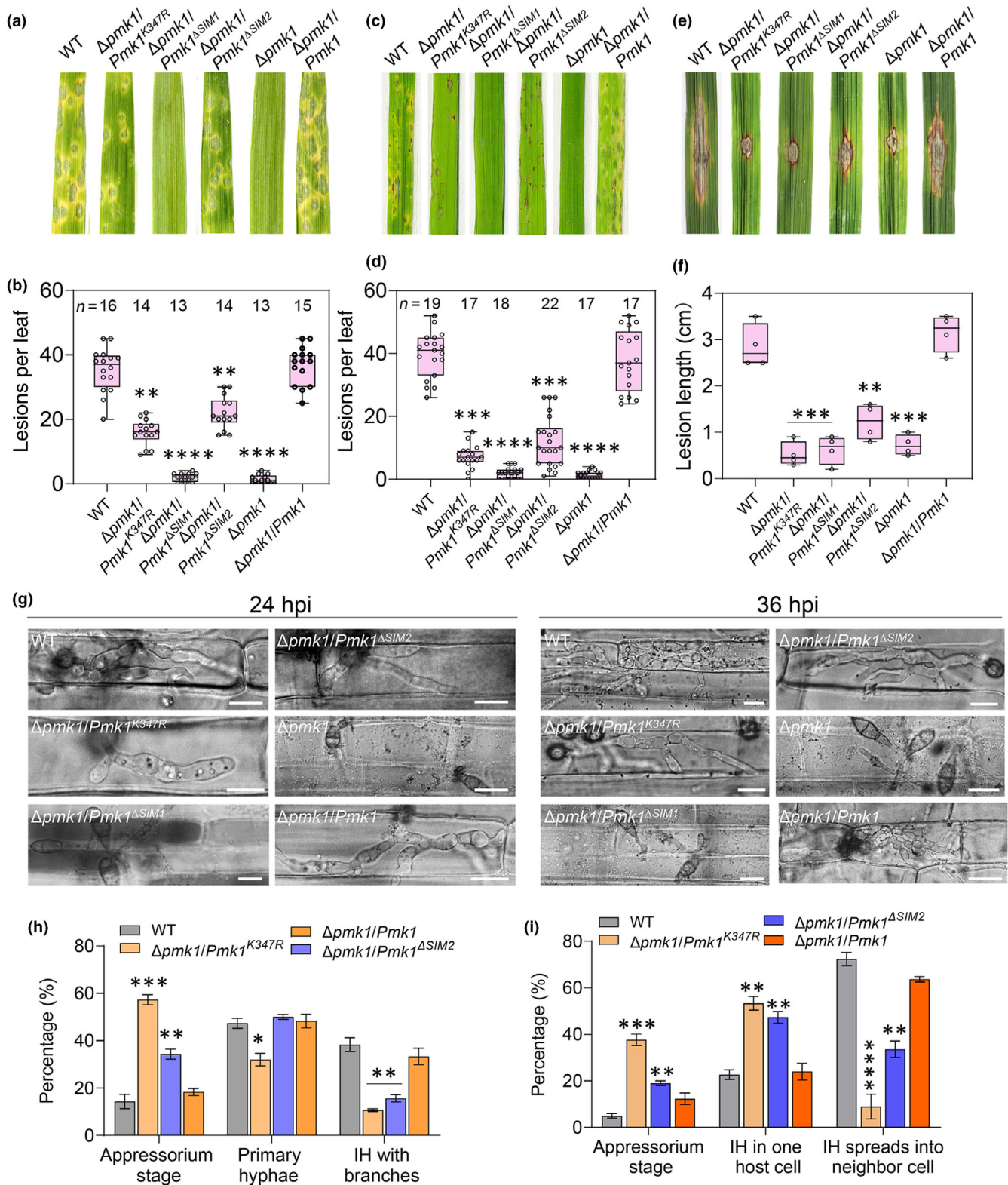
Fig. 7 Sumoylation of Pmk1 regulates the virulence of *Magnaporthe oryzae*. (a) Disruption of Pmk1 sumoylation results in reduced virulence on barley leaves. Conidia from the indicated strains were sprayed onto leaves at a concentration of 3×10^4 conidia ml^{-1}, and lesions were observed at 5 d post inoculation (dpi). (b) The number of lesions shown in (a) was quantified. (c) Disruption of Pmk1 sumoylation leads to attenuated virulence on rice leaves. Conidia from the indicated strains were sprayed at a concentration of 1.5×10^5 conidia ml^{-1}, and the formation of lesions was assessed at 5 dpi. (d) The number of lesions shown in (b) was quantified. (e) Reduced invasive growth of Pmk1 sumoylation-disrupted strains on wounded rice leaves. Mycelia blocks were inoculated onto wounded leaves, and growth was observed at 4 dpi. (f) Diameters of disease lesions on wounded leaves depicted in (e) were measured. (g) Observation of the infection process in barley epidermal cells at 24 h post inoculation (hpi). Conidia were injected into rice leaf sheaths, and the infection structures were microscopically observed at 24 and 36 hpi. The bar represents 10 μm. (h) The formation ratio of primary invasive hyphae in rice sheaths at 24 hpi was determined. (i) The formation ratio of invasive hyphae (IH) spreading cell-to-cell in rice sheaths at 36 hpi was assessed. Data are presented as mean ± SE from three independent replicates and were analyzed by two-way ANOVA followed by Tukey's test, with asterisks indicating significant differences (**, $P < 0.01$; ***, $P < 0.001$; ****, $P < 0.0001$).

suggesting that sumoylation may not affect the nuclear localization of Pmk1 for its role in regulating downstream targets.

Sumoylation of Pmk1 is essential for infection of *M. oryzae*

Importantly, what concerns us is whether the sumoylation of Pmk1 can be involved in the regulation of the biological function of the rice blast fungus. Biological phenotype analysis indicated that there was no difference in the growth rate among the $\Delta pmk1/Pmk1$, $\Delta pmk1/Pmk1^{K347R}$, $\Delta pmk1$, and $\Delta smt3/Pmk1$ strains (Fig. S6a,b). The $\Delta pmk1/Pmk1^{K347R}$-GFP strains exhibited darker colony morphology and increased sporulation, whereas the $\Delta pmk1$ strains displayed white colony morphology and had slightly reduced sporulation (Fig. S6a–d). We then examined the effect of the sumoylation of Pmk1 on the infection of the rice blast fungus. Conidia collected from WT, $\Delta pmk1/Pmk1$, $\Delta pmk1/Pmk1^{K347R}$, $\Delta pmk1/Pmk1^{\Delta SIM1}$, $\Delta pmk1/Pmk1^{\Delta SIM2}$, and $\Delta pmk1$ were used to incubate the susceptible barley and rice. In the leaf spray experiment, $\Delta pmk1/Pmk1^{K347R}$ and $\Delta pmk1/Pmk1^{\Delta SIM2}$ displayed decreased disease lesions compared with WT and $\Delta pmk1/Pmk1$ on barley (Fig. 7a,b) and rice (Fig. 7c,d), while $\Delta pmk1/Pmk1^{\Delta SIM1}$ and $\Delta pmk1$ failed to produce any leaf lesions. Similar results were also observed when the mycelial blocks of the above strains were inoculated on wounded rice leaves (Fig. 7e,f).

To further determine why the strains with Pmk1 sumoylated mutations exhibited attenuated virulence, we observed the cellular infection processes in the rice sheath. At 24 hpi, the $\Delta pmk1/Pmk1^{\Delta SIM1}$, like the $\Delta pmk1$ strain, failed to form any appressorium, while *c.* $30 \pm 0.5\%$ of the appressoria in $\Delta pmk1/Pmk1^{K347R}$ formed primary IH compared with WT ($49 \pm 1.8\%$), $\Delta pmk1/Pmk1^{\Delta SIM2}$ ($49 \pm 1.8\%$), and the complement strain $\Delta pmk1/Pmk1$ ($50 \pm 1.26\%$; Fig. 7g,h). At 36 hpi, we surprisingly discovered that $\Delta pmk1/Pmk1^{K347R}$ was more likely to be trapped in a single plant cell but WT and the complement strain successfully spread into neighboring cells through cell-to-cell movement (Fig. 7g,i). Altogether, we concluded that the sumoylation of Pmk1 plays a crucial role in host penetration and invasive hyphae growth.

Sumoylation of Pmk1 is required for functional appressorium development

The activation of the Pmk1-MAPK signaling pathway is essential for appressorium formation (Xu & Hamer, 1996; Osés-Ruiz

et al., 2017). Infection process observation revealed the attenuated penetration ability of $\Delta pmk1/Pmk1^{K347R}$, but the appressorium formation rate was not affected (Fig. S6e), suggesting sumoylation of Pmk1 at K347 is important for appressorial maturation. Interestingly, the conidia of $\Delta pmk1/Pmk1^{K347R}$ mutants can form appressoria on hydrophilic surfaces (Fig. 8a,b), and the mycelium of $\Delta pmk1/Pmk1^{K347R}$ mutants is more likely to form hyphopodia on hydrophobic surfaces (Fig. 8a,c). Furthermore, the $\Delta pmk1/Pmk1^{K347R}$ mutants also tend to form double appressoria in a single conidium (Fig. 8d,e). A similar result was found previously in the continuously activated Pmk1 mutants (Qi *et al.*, 2015), which is consistent with the above conclusion that sumoylation suppresses the phosphorylation of Pmk1.

After treatment of 8% glycerol for 30 min, we found there were 63% (± 1.76) of appressoria collapse in $\Delta pmk1/Pmk1^{K347R}$, much higher than that in P131 (32% $\pm$ 1.26) and the complement strain (37% $\pm$ 1.00; Fig. 8f,g). These data indicated that the accumulation of appressorial turgor was severely reduced in $\Delta pmk1/Pmk1^{K347R}$. Glycogen and lipid droplet staining assays revealed that the utilization of conidial nutrient storages was much quicker during the appressoria maturation process of $\Delta pmk1/Pmk1^{K347R}$ in comparison with WT (Figs 8h,i, S7a,b). Accelerated nutrient utilization during the formation of appressorium may indicate defects in cellular autophagy during this process, so the autophagy level of ATG8-GFP during appressoria formation was observed by fluorescence microscope. The amount of ATG8-GFP-labeled autophagosomes was much more in the hyphae and appressorial formation of $\Delta pmk1/Pmk1^{K347R}$ than that of the WT, thus resulting in faster autophagy once induced by nitrogen starvation in $\Delta pmk1$/Pmk1^{K347R} (Fig. 8j–n). These data confirmed that one of the reasons for the weakened pathogenicity of $\Delta pmk1/Pmk1^{K347R}$ is the insufficient accumulation of appressorial turgor caused by abnormal nutrient utilization during the maturation of appressorium, resulting in a decrease in penetration to host plants. *M. oryzae* appressoria normally form a septin ring to accumulate an actin ring for penetration (Dagdas *et al.*, 2012); interestingly, the $\Delta pmk1/Pmk1^{K347R}$ mutants tended to form granule structures but not septin rings (Fig. 8o,p), suggesting sumoylation of Pmk1 is required for septin ring assembling.

Discussion

In plant pathogenic fungi, the Pmk1-MAPK signaling pathway is crucial for infection, particularly in the differentiation of

infection structures like appressoria (Xu & Hamer, 1996; Di Pietro *et al.*, 2001; Sakulkoo *et al.*, 2018). Although the main components of this pathway are well known in various fungi, the regulation of its central component, Pmk1, remains unclear. Our study reveals the vital role of the interplay between sumoylation and phosphorylation in Pmk1's function. We demonstrate that sumoylation suppresses Pmk1 phosphorylation, acting as a feedback mechanism similar to a braking system that prevents
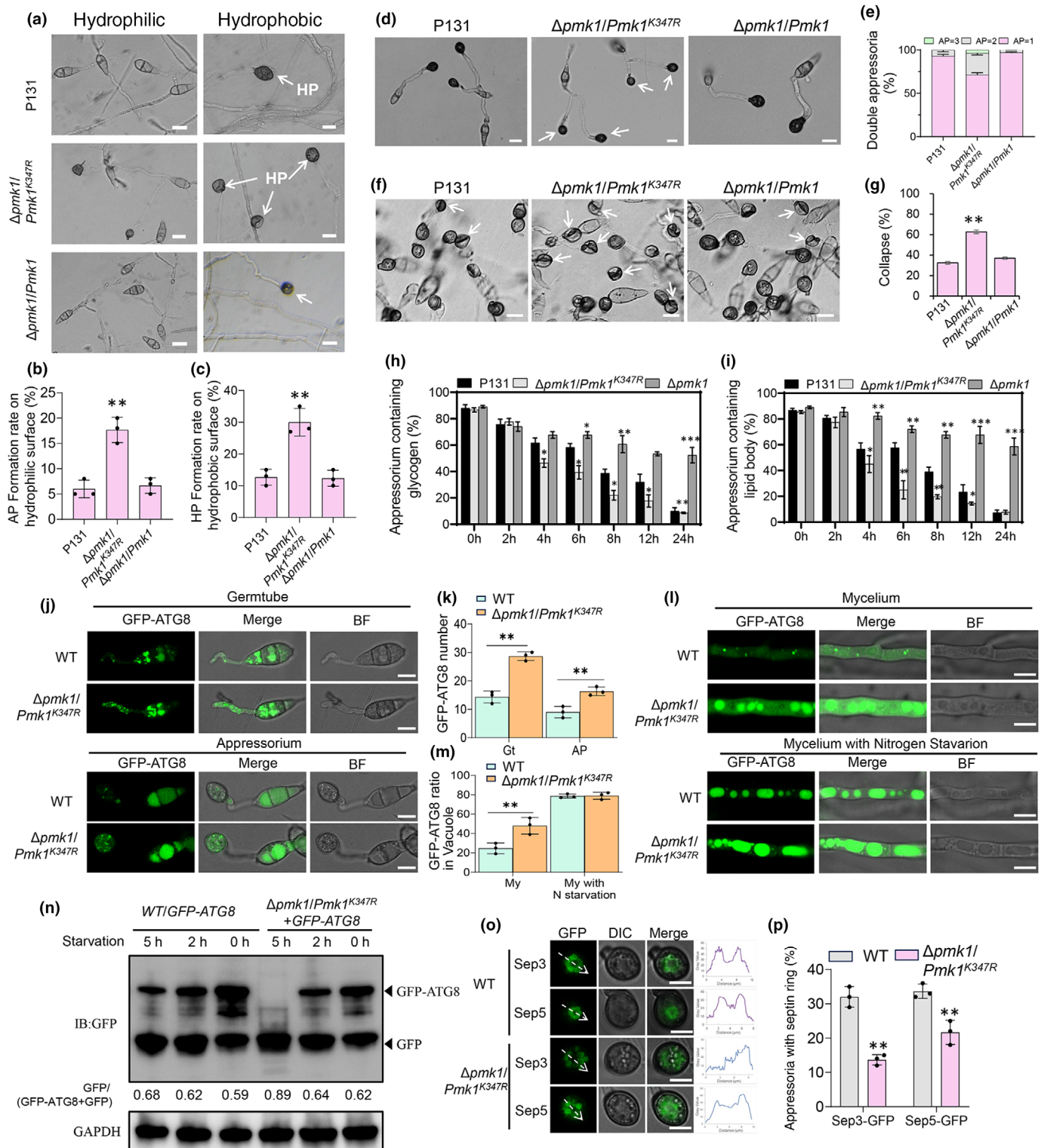
Fig. 8 Sumoylated Pmk1 regulates appressorium function in *Magnaporthe oryzae*. (a) Observation of hyphopodium (HP) and appressorium formation in Pmk1 sumoylation disruption strains on a hydrophobic surface. Arrows indicate HP. Bar, 10 μm. (b) Statistical analysis of appressorium formation rate on hydrophilic surfaces from observations in (a). (c) Statistical analysis of HP formation rate on hydrophobic surfaces from observations in (a). (d) Appressorium formation in Pmk1 sumoylation disruption strains on hydrophobic surfaces at 18 hpi. White arrow indicates appressorium. Bar, 10 μm. (e) Statistical analysis of appressorium formation, with AP = 1 and AP = 2 representing the number of appressoria formed per conidium. (f) Turgor pressure measurement in appressoria of Pmk1 sumoylated mutations after treatment with 8% glycerol. White arrows point to collapsed appressoria. Bar, 10 μm. (g) Statistical analysis of the ratio of collapsed appressoria. (h) Quantitative analysis of lipid body formation during appressorium formation in the indicated strains, stained with KI/I$_2$ solution. (i) Quantitative analysis of lipid body formation in conidia stained with Nile Red. (j) Observation of GFP-ATG8 autophagosomes in germtube and appressoria of the strains with disrupted Pmk1 sumoylation. (k) The number of GFP-ATG8-labeled autophagosomes during appressorium development. (l) Observation of ATG8-GFP autophagosomes in wild-type (WT) and Δpmk1/Pmk1^{K347R} under nitrogen starvation. (m) Autophagy intensity assessed by the proportion of GFP-Atg8 translocated to vacuoles. (n) Immunoblotting detection of ATG8-GFP under nitrogen starvation conditions, with anti-GAPDH as a loading control. The numbers below each lane indicate the ratio of free GFP to the total amount of intact GFP-Atg8 and free GFP. (o) Subcellular localization of septins in WT and Δpmk1/Pmk1^{K347R} strains during appressorial formation at 24 hpi, visualized with Sep3-GFP and Sep5-GFP under confocal microscopy. (p) Percentage of appressoria with intact septin rings from observations in (o). Data (b, c, g, h, i, k and m) are presented as mean ± SE from three independent replicates and were analyzed by two-way ANOVA followed by Tukey's test, with asterisks indicating significant differences (*, $P < 0.05$; **, $P < 0.01$; ***, $P < 0.001$).

excessive phosphorylation. This ensures the precise regulation of the Pmk1-MAPK signaling pathway during appressorium-mediated infection of *M. oryzae*.

Sumoylation serves as a critical feedback mechanism for the Pmk1-MAPK signaling pathway in *M. oryzae*, ensuring precise regulation during appressorium formation to prevent overactivation. This conclusion is supported by several key findings. First, sumoylation of Pmk1 is dynamically regulated during infection, being highly active in hyphae but less so during infection, indicating its adaptive regulatory role in fungal development (Fig. 1b). Second, sumoylation at K347 suppresses Pmk1 phosphorylation by modulating its interaction with the kinase Mst7, as evidenced by various experimental assays (Figs 4e–h, S4a,b). Third, sumoylation specifically inhibits Pmk1 phosphorylation without affecting its subcellular localization or stability, highlighting its role in fine-tuning Pmk1 activity (Figs 4a–d, S5). Fourth, sumoylation-deficient mutants exhibit increased phosphorylation of downstream targets like Mst12 and overexpression of appressorium-related genes, demonstrating the impact of sumoylation on the signaling output of the Pmk1-MAPK pathway (Fig. 6). The conservation of sumoylation sites and motifs across plant pathogenic fungi suggests this regulatory mechanism is widespread (Fig. 1c). Sumoylation mutants show defects in appressorium function, including increased autophagy, reduced turgor accumulation, and impaired septin ring formation, which are critical for successful infection (Fig. 8). This control mechanism likely stops overactivation, which could cause multiple appressoria to form from one conidium. This is shown by the Δ*pmk1*/*Pmk1*^{K347R} mutant's traits (Fig. 8a,d,e). Together, these findings establish sumoylation as a crucial feedback mechanism that prevents overactivation of the Pmk1-MAPK pathway during appressorium formation in *M. oryzae*.

Our study suggests that sumoylation regulates Pmk1 phosphorylation by changing its structure, thus influencing its interaction with the kinase Mst7. Structural analysis reveals that sumoylation-induced conformational changes in Pmk1 disrupt its interaction interface with Mst7, providing a structural basis for the feedback regulation (Fig. 5). We mutated the sumoylation site (Pmk1^{K347R}) and found that this mutation significantly enhanced the interaction between Pmk1 and Mst7 in Y2H, Co-

IP, and BiFC assays. Removing the SUMOylation interaction motifs (SIM1 or SIM2) also strengthened this interaction. Structural analysis identified Ile85 in the SIM1 domain as the interaction site between Pmk1 and Smt3, and Y2H assays with Pmk1 mutants confirmed that mutating Ile85 weakens this interaction (Fig. S2). Furthermore, the SUMOylation site mutation (Pmk1^{K347R}) increased Pmk1 and downstream Mst12 phosphorylation, indicating that sumoylation suppresses Pmk1 phosphorylation. In summary, our findings show that sumoylation of Pmk1 at K347 suppresses its phosphorylation and that the Ile85 site in SIM1 is crucial for the Pmk1–Smt3 interaction, enhancing our understanding of this regulatory process.

In typical cellular regulation, phosphorylation is balanced by phosphatase-mediated dephosphorylation. We initially hypothesized that SUMOylation of Pmk1, which restrains its phosphorylation, might enhance its interaction with the phosphatase Pmp1 and diminish its interaction with the kinase Mst7. However, our experimental findings revealed an unexpected outcome. We observed that SUMOylation of Pmk1 inhibits its interaction with both Pmp1 and Mst7 (Fig. 4e–l). This seemingly paradoxical result can be interpreted through structural insights. Given that Pmp1 and Mst7 compete for the same phosphorylation site, SUMOylation-induced conformational changes in Pmk1 likely hinder its binding to both Mst7 and Pmp1. This represents a spatial antagonism between SUMOylation and phosphorylation, distinct from the site-based antagonism between Pmp1 and Mst7.

In the conidial stage of *M. oryzae*, the Pmk1-MAPK signaling is not induced; both SUMOylation and Pmk1 protein levels are low (Fig. 1b; Li *et al.*, 2012). Upon germination to form appressoria, the Pmk1-MAPK signaling is activated; both Pmk1 levels and phosphorylation increase significantly. While Pmp1 functions to inhibit Pmk1 phosphorylation and prevent overactivation, SUMOylation's inhibitory effect on Pmk1 phosphorylation during appressorium formation remains biologically significant. During this critical stage, the fungus must precisely regulate Pmk1 activity for environmental adaptation and cell morphogenesis. As a post-translational modification, we proposed that SUMOylation offers a rapid and flexible regulatory mechanism by modulating Pmk1 activity without altering its abundance. Appressorium formation, a highly coordinated
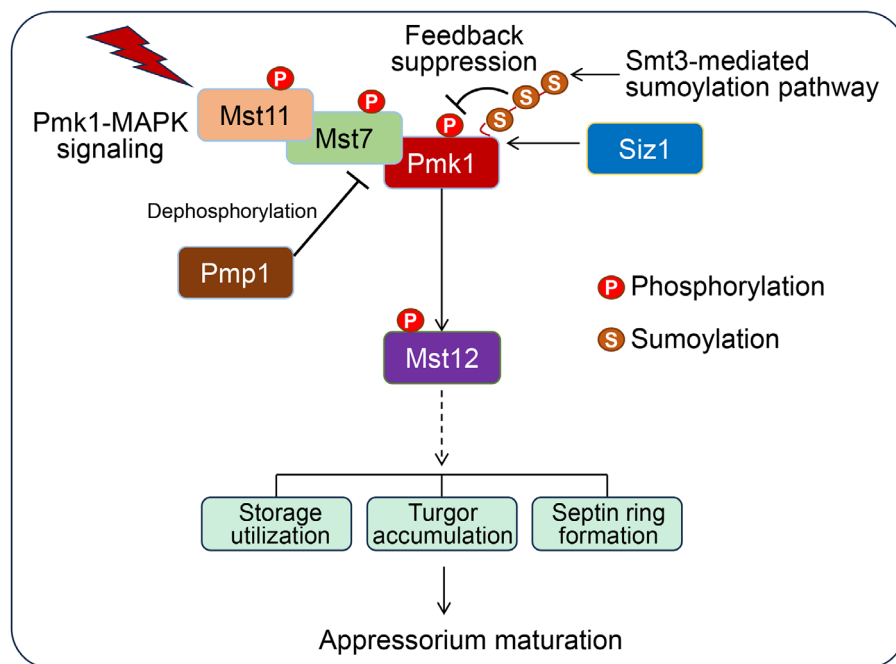
Fig. 9 Proposed model for Pmk1 function regulated by sumoylation. Smt3-mediated sumoylation of Pmk1 is shown to inhibit its phosphorylation by influencing the interaction between Pmk1 and Mst7. This modulation leads to a fine-tuned Pmk1-MAPK signaling pathway. Consequently, the coordinated phosphorylation of Mst12 facilitates the appropriate gene expression required for regulating appressorium maturation and invasive growth, which are essential for the infection process of *Magnaporthe oryzae*. MAPK, mitogen-activated protein kinase. Dashed arrows indicate indirect regulation, solid arrows indicate direct regulation, and blunt-ended arrows indicate inhibitory regulation.

process involving multiple interacting signaling pathways, may see SUMOylation interact with other signaling components. By inhibiting Pmk1 phosphorylation, SUMOylation fine-tunes the signaling output, ensuring normal appressorium formation and function.

Another Pmk1 regulatory factor is Rnc1, which stabilizes Pmp1 mRNA, a phosphatase that counteracts Pmk1 phosphorylation (Taga *et al.*, 2010). While Rnc1 fine-tunes the pathway post-transcriptionally, sumoylation adds another regulatory layer. Unlike Rnc1, sumoylation does not directly promote dephosphorylation but modulates Pmk1's phosphorylation state by altering its protein structure. This modification potentially disrupts the binding of kinases and phosphatases to Pmk1, influencing its phosphorylation level and the subsequent activation of downstream factors like Mst12. We propose a model where Smt3 - mediated sumoylation of Pmk1 adjusts its interaction with Mst7, thereby inhibiting excessive phosphorylation and coordinating the gene expression vital for appressorium maturation and *M. oryzae*'s invasive growth, without relying on Pmp1's dephosphorylation activity (Fig. 9).

Sumoylation's role in modulating phosphorylation is conserved across organisms, exemplified by its inhibitory effect on mammalian AMPKα1 activation and its impact on kinase activity and protein stability (Yan *et al.*, 2015). Interestingly, sumoylation can also enhance kinase activity, as seen with ERK5's nuclear translocation and PYK2's autophosphorylation (Erazo *et al.*, 2020), highlighting the diverse outcomes of sumoylation in cellular regulation. The crosstalk between sumoylation and phosphorylation is a well-studied phenomenon, particularly in the context of MAPK pathways and their influence on key transcription factors like STAT1, ATF7, c-Fos, and Elk-1 (Camuzeaux *et al.*, 2008; Yang & Sharrocks, 2010; Heo *et al.*, 2013). Sumoylation generally inhibits the activity of these transcription factors.

Recent research has revealed that Pmk1 regulates diverse processes, including nutrient utilization, appressorial ring formation, invasive hyphal extension, and effector protein secretion (Park *et al.*, 2002; Sakulkoo *et al.*, 2018; Cruz-Mireles *et al.*, 2024). Our findings show that the K347 SUMO site mutation in Pmk1 results in multiple appressoria formation and reduced virulence, likely due to insufficient nutrient reserves in conidia to support the development of multiple functional appressoria. Data indicate that genetic complementation in Δ*pmk1* mutants with overexpressed Pmk1 fails to fully restore virulence, underscoring the necessity of precise Pmk1 expression levels. When sumoylation is inhibited, Pmk1 becomes hyperactivated, leading to accelerated nutrient utilization, enhanced phosphorylation of downstream targets, and overexpression of downstream substrates. These observations are consistent with our results showing faster nutrient consumption during appressorium formation (Figs 8h,i, S7a,b), increased ATG8-labeled autophagosomes (Fig. 8j–n), and stronger phosphorylation of Mst12 in the Pmk1^{K347R} mutants (Fig. 6c).

The Pmk1 MAPK pathway is a key focus in fungal biology and plant pathology due to its crucial role in plant infection. The high conservation of the K347 site and SIM motifs among plant pathogenic fungi suggests that Pmk1 sumoylation is a widespread regulatory mechanism with implications for various infection processes. While Pmk1 is a promising target for fungicides, its ubiquity poses challenges for developing targeted treatments. Our research advocates for the targeting of Pmk1's post-translational modifications to enhance the efficacy and specificity of antifungal therapies.

Acknowledgements

Key Laboratory of High Technology for Plant Protection (zhizhong2025-03) and post-doctoral innovation research positions in Hubei Province.

Competing interests

None declared.

Author contributions

CL contributed to the conceptualization, resources, formal analysis, investigation, methodology, writing – original draft, and writing – review and editing. HH contributed to the investigation, methodology, writing – original draft, and writing – review and editing. XC and JZ contributed to the investigation and methodology. JJ contributed to the investigation – assessed the molecular docking. JZ, ZJ, YK and ZR contributed to the investigation. JS and SC contributed to the supervision, writing – review and editing, and resources. HL, LZ and JH contributed to the supervision, and writing – review and editing. X-LC contributed to the conceptualization, resources, data curation, formal analysis, supervision, funding acquisition, visualization, writing – original draft, project administration, writing – review and editing. CL and HH contributed equally to this work.

ORCID

Xiao-Lin Chen https://orcid.org/0000-0002-5492-516X
Caiyun Liu https://orcid.org/0000-0001-6825-3977
Lu Zheng https://orcid.org/0000-0002-2414-1671

Data availability

All data collected to support this study are available in the article and the Supporting Information (Figs S1–S7; Tables S1–S3).

References

Abramson J, Adler J, Dunger J, Evans R, Green T, Pritzel A, Ronneberger O, Willmore L, Ballard AJ, Bambrick J *et al.* **2024.** Accurate structure prediction of biomolecular interactions with AlphaFold 3. *Nature* **630**: 493–500.

Bruno KS, Tenjo F, Li L, Hamer JE, Xu JR. 2004. Cellular localization and role of kinase activity of PMK1 in *Magnaporthe grisea*. *Eukaryotic Cell* **3**: 1525–1532.

Camuzeaux B, Diring J, Hamard PJ, Oulad-Abdelghani M, Donzeau M, Vigneron M, Kedinger C, Chatton B. 2008. p38beta2-mediated phosphorylation and sumoylation of ATF7 are mutually exclusive. *Journal of Molecular Biology* **384**: 980–991.

Cruz-Mireles N, Osés-Ruiz M, Derbyshire P, Jégousse C, Ryder LS, Bautista MJA, Eseola A, Sklenar J, Tang B, Yan X *et al.* **2024.** The phosphorylation landscape of infection-related development by the rice blast fungus. *Cell* **187**: 2557–2573.

Dagdas YF, Yoshino K, Dagdas G, Ryder LS, Bielska E, Steinberg G, Talbot NJ. 2012. Septin-mediated plant cell invasion by the rice blast fungus, *Magnaporthe oryzae*. *Science* **336**: 1590–1595.

Di Pietro A, García-MacEira FI, Méglecz E, Roncero MI. 2001. A MAP kinase of the vascular wilt fungus *Fusarium oxysporum* is essential for root penetration and pathogenesis. *Molecular Microbiology* **39**: 1140–1152.

Erazo T, Espinosa-Gil S, Diéguez-Martínez N, Gómez N, Lizcano JM. 2020. Sumoylation is required for ERK5 nuclear translocation and ERK5-mediated cancer cell proliferation. *International Journal of Molecular Sciences* **21**: 2203.

Filosa G, Barabino SM, Bachi A. 2013. Proteomics strategies to identify SUMO targets and acceptor sites: a survey of RNA-binding proteins SUMOylation. *Neuromolecular Medicine* **15**: 661–676.

Gareau JR, Lima CD. 2010. The SUMO pathway: emerging mechanisms that shape specificity, conjugation and recognition. *Nature Reviews. Molecular Cell Biology* **11**: 861–871.

Geiss-Friedlander R, Melchior F. 2007. Concepts in sumoylation: a decade on. *Nature Reviews. Molecular Cell Biology* **8**: 947–956.

Giraldo MC, Dagdas YF, Gupta YK, Mentlak TA, Yi M, Martinez-Rocha AL, Saitoh H, Terauchi R, Talbot NJ, Valent B. 2013. Two distinct secretion systems facilitate tissue invasion by the rice blast fungus *Magnaporthe oryzae*. *Nature Communications* **4**: 1996.

Heo KS, Chang E, Takei Y, Le NT, Woo CH, Sullivan MA, Morrell C, Fujiwara K, Abe J. 2013. Phosphorylation of protein inhibitor of activated STAT1 (PIAS1) by MAPK-activated protein kinase-2 inhibits endothelial inflammation via increasing both PIAS1 transrepression and SUMO E3 ligase activity. *Arteriosclerosis, Thrombosis, and Vascular Biology* **33**: 321–329.

Jian Y, Chen X, Sun K, Liu Z, Cheng D, Cao J, Liu J, Cheng X, Wu L, Zhang F *et al.* **2023.** SUMOylation regulates pre-mRNA splicing to overcome DNA damage in fungi. *New Phytologist* **237**: 2298–2315.

Kolesar P, Sarangi P, Altmannova V, Zhao X, Krejci L. 2012. Dual roles of the SUMO-interacting motif in the regulation of Srs2 sumoylation. *Nucleic Acids Research* **40**: 7831–7843.

Li G, Zhou X, Xu JR. 2012. Genetic control of infection-related development in *Magnaporthe oryzae*. *Current Opinion in Microbiology* **15**: 678–684.

Li X, Gao C, Li L, Liu M, Yin Z, Zhang H, Zheng X, Wang P, Zhang Z. 2017. MoEnd3 regulates appressorium formation and virulence through mediating endocytosis in rice blast fungus *Magnaporthe oryzae*. *PLoS Pathogens* **13**: e1006449.

Liu C, Li Z, Xing J, Yang J, Wang Z, Zhang H, Chen D, Peng YL, Chen XL. 2018. Global analysis of sumoylation function reveals novel insights into development and appressorium-mediated infection of the rice blast fungus. *New Phytologist* **219**: 1031–1047.

Liu C, Liu T, Lv Z, Qin M, Qu Z, Zhang Z, Li F, Chen D, Zhang X, Chen XL *et al.* **2022.** A calcineurin regulator MoRCN1 is important for asexual development, stress response, and plant infection of *Magnaporthe oryzae*. *Frontiers in Plant Science* **13**: 925645.

Liu W, Triplett L, Chen XL. 2021. Emerging roles of posttranslational modifications in plant-pathogenic fungi and bacteria. *Annual Review of Phytopathology* **59**: 99–124.

Menke FL, Kang HG, Chen Z, Park JM, Kumar D, Klessig DF. 2005. Tobacco transcription factor WRKY1 is phosphorylated by the MAP kinase SIPK and mediates HR-like cell death in tobacco. *Molecular Plant–Microbe Interactions* **18**: 1027–1034.

Osés-Ruiz M, Cruz-Mireles N, Martin-Urdiroz M, Soanes DM, Eseola AB, Tang B, Derbyshire P, Nielsen M, Cheema J, Were V *et al.* **2021.** Appressorium-mediated plant infection by *Magnaporthe oryzae* is regulated by a Pmk1-dependent hierarchical transcriptional network. *Nature Microbiology* **6**: 1383–1397.

Osés-Ruiz M, Sakulkoo W, Littlejohn GR, Martin-Urdiroz M, Talbot NJ. 2017. Two independent S-phase checkpoints regulate appressorium-mediated plant infection by the rice blast fungus *Magnaporthe oryzae*. *Proceedings of the National Academy of Sciences, USA* **114**: E237–e244.

Park G, Xue C, Zheng L, Lam S, Xu JR. 2002. MST12 regulates infectious growth but not appressorium formation in the rice blast fungus *Magnaporthe grisea*. *Molecular Plant - Microbe Interactions* **15**: 183–192.

Qi L, Kim Y, Jiang C, Li Y, Peng Y, Xu JR. 2015. Activation of Mst11 and feedback inhibition of germ tube growth in *Magnaporthe oryzae*. *Molecular Plant - Microbe Interactions* **28**: 881–891.

Sakulkoo W, Osés-Ruiz M, Oliveira Garcia E, Soanes DM, Littlejohn GR, Hacker C, Correia A, Valent B, Talbot NJ. 2018. A single fungal MAP kinase

controls plant cell-to-cell invasion by the rice blast fungus. *Science* 359: 1399–1403.

Shao W, Sun K, Ma T, Jiang H, Hahn M, Ma Z, Jiao C, Yin Y. 2023. SUMOylation regulates low-temperature survival and oxidative DNA damage tolerance in *Botrytis cinerea*. *New Phytologist* 238: 817–834.

Song J, Durrin LK, Wilkinson TA, Krontiris TG, Chen Y. 2004. Identification of a SUMO-binding motif that recognizes SUMO-modified proteins. *Proceedings of the National Academy of Sciences, USA* 101: 14373–14378.

Taga A, Satoh R, Ishiwata S, Kodama S, Sato A, Suzuki K, Sugiura R. 2010. *In vitro* assay of the interaction between Rnc1 protein and Pmp1 mRNA by affinity capillary electrophoresis with a carboxylated capillary. *Journal of Pharmaceutical and Biomedical Analysis* 53: 1332–1337.

Talbot NJ. 2003. On the trail of a cereal killer: Exploring the biology of *Magnaporthe grisea*. *Annual Review of Microbiology* 57: 177–202.

Thines E, Weber RW, Talbot NJ. 2000. MAP kinase and protein kinase A-dependent mobilization of triacylglycerol and glycogen during appressorium turgor generation by *Magnaporthe grisea*. *Plant Cell* 12: 1703–1718.

Turrà D, Segorbe D, Di Pietro A. 2014. Protein kinases in plant-pathogenic fungi: conserved regulators of infection. *Annual Review of Phytopathology* 52: 267–288.

Wilson RA, Talbot NJ. 2009. Under pressure: investigating the biology of plant infection by *Magnaporthe oryzae*. *Nature Reviews. Microbiology* 7: 185–195.

Xu JR. 2000. Map kinases in fungal pathogens. *Fungal Genetics and Biology* 31: 137–152.

Xu JR, Hamer JE. 1996. MAP kinase and cAMP signaling regulate infection structure formation and pathogenic growth in the rice blast fungus *Magnaporthe grisea*. *Genes & Development* 10: 2696–2706.

Yan Y, Ollila S, Wong IPL, Vallenius T, Palvimo JJ, Vaahtomeri K, Mäkelä TP. 2015. SUMOylation of AMPKα1 by PIAS4 specifically regulates mTORC1 signalling. *Nature Communications* 6: 8979.

Yang SH, Sharrocks AD. 2010. MAP kinase: SUMO pathway interactions. *Methods in Molecular Biology* 661: 343–367.

Zhang H, Yang J, Liu M, Xu X, Yang L, Liu X, Peng Y, Zhang Z. 2024. Early molecular events in the interaction between *Magnaporthe oryzae* and rice. *Phytopathology Research* 6: 9.

Zhang X, Wang Z, Jiang C, Xu JR. 2021. Regulation of biotic interactions and responses to abiotic stresses by MAP kinase pathways in plant pathogenic fungi. *Stress Biology* 1: 5.

Supporting Information

Additional Supporting Information may be found online in the Supporting Information section at the end of the article.

Fig. S1 Siz1 is required for sumoylation of Pmk1 in *Magnaporthe oryzae*.

Fig. S2 Yeast two-hybrid assay demonstrates the interaction between Pmk1[I85A] and Smt3(GG).

Fig. S3 Phosphorylation levels of Pmk1 during the appressorium formation of *M. oryzae*.

Fig. S4 Co-immunoprecipitation of Mst7 and Pmk1 sumoylation mutations.

Fig. S5 Subcellular localization of Pmk1 during infection in different strains.

Fig. S6 Biological phenotype analysis of experimental strains.

Fig. S7 Glycogen and lipid utilization during appressorium maturation.

Table S1 Fungal strains used in this study.

Table S2 Plasmids used in this study.

Table S3 Primers used in this study.